Best
Available
Copy

AD-761 625

NOVEL SURFACE ACOUSTIC WAVE TRANS-
DUCER TECHNIQUES

Eugene R. Westerberg, et al

Stanford Research Institute

Prepared for:

Defense Advanced Research Projects Agency

April 1973

Final Report

NOVEL SURFACE ACOUSTIC
WAVE TRANSDUCER TECHNIQUES

By: E. R. WESTERBERG   ROBERT E. LEE

Prepared for:

DEFENSE ADVANCED RESEARCH PROJECTS AGENCY
1400 WILSON BOULEVARD
ARLINGTON, VIRGINIA 22209

Attention: DR. MARTIN STICKLEY
                     MATERIALS SCIENCES

CONTRACT DAHC15-72-C-0265

STANFORD RESEARCH INSTITUTE
Menlo Park, California 94025 · U.S.A.

59

STANFORD RESEARCH INSTITUTE
Menlo Park, California 94025 · U.S.A.

Final Report

April 1973

NOVEL SURFACE ACOUSTIC
WAVE TRANSDUCER TECHNIQUES

By: E. R. WESTERBERG   ROBERT E. LEE

Prepared for:

DEFENSE ADVANCED RESEARCH
  PROJECTS AGENCY
1400 WILSON BOULEVARD
ARLINGTON, VIRGINIA 22209

Attention: DR. MARTIN STICKLEY
             MATERIALS SCIENCES

CONTRACT DAHC15-72-C-0265

SRI Project 1909

DARPA Order 2198
Program Code No. S0507A
Contract DAHC15-72-C-0265
Effective Date: May 1, 1972
Contract Expiration: Dec. 31, 1972
Amount of Contract: $59,215.00
Principal Investigator:
    E. R. Westerberg
    (415) 326-6200 Ext. 4120

Approved by:

F. J. KAMPHOEFNER, *Director*
Engineering Sciences Laboratory

BONNAR COX, *Executive Director*
Information Science and Engineering Division

DOCUMENT CONTROL DATA - R & D

Security classification of title, body of abstract and indexing annotation must be entered when the overall report is classified)

1. ORIGINATING ACTIVITY (Corporate author)	2a. REPORT SECURITY CLASSIFICATION
Stanford Research Institute	UNCLASSIFIED
333 Ravenswood Avenue	2b. GROUP
Menlo Park, California 94025	

3. REPORT TITLE

NOVEL SURFACE ACOUSTIC WAVE TRANSDUCER TECHNIQUES

4. DESCRIPTIVE NOTES (Type of report and inclusive dates)

Final Report

5. AUTHOR(S) (First name, middle initial, last name)

Eugene R. Westerberg   Robert E. Lee

6. REPORT DATE	7a. TOTAL NO. OF PAGES	7b. NO. OF REFS
April 1973		11

8a. CONTRACT OR GRANT NO.	9a. ORIGINATOR'S REPORT NUMBER(S)
Contract DAHC15-72-C-0265	Final Report
b. PROJECT NO.	SRI Project 1909
DARPA Order 2198	
c.	9b. OTHER REPORT NO(S) (Any other numbers that may be assigned this report)
Program Code No. 50507A	
d. None	

10. DISTRIBUTION STATEMENT

11. SUPPLEMENTARY NOTES	12. SPONSORING MILITARY ACTIVITY
	Defense Advanced Research Projects Agency
	1400 Wilson Boulevard
	Arlington, Virginia 22209

13. ABSTRACT

    This research demonstrates that a new electron-beam image projection exposure technique, the "slit-lens", can be applied to the fabrication of high resolution interdigital patterns for use as high frequency surface acoustic wave transducers. Further research efforts include the development of the ancillary thin-film techniques for making metallic patterns on piezoelectric substrates, and the design, fabrication, and electrical test of actual surface acoustic wave delay lines produced by the foregoing techniques.

Details of illustrations in this
document may be better studied
on microfiche.

DD FORM 1473 (PAGE 1)
1 NOV 65

S/N 0101-807-6801

i

KEY WORDS	LINK A		LINK B		LINK C	
	ROLE	WT	ROLE	WT	ROLE	WT
Slit-lens						
Transducer						
Acoustic wave						
Exposure systems						

DD FORM 1473 (BACK)
1 NOV 65
(PAGE 2)

1a.

UNCLASSIFIED
Security Classification

CONTENTS

Preceding page blank

ILLUSTRATIONS

TABLES

Preceding page blank

SUMMARY

As the interest grows in making higher and higher frequency surface acoustic wave devices such as delay lines, frequency filters, and complex digital and analog matched filters, the technology is forced to deal with smaller and smaller dimensions. At frequencies above about 1 GHz the width of an average transducer finger drops into the submicron region, and conventional photolithographic techniques are not adequate in this domain. Photolithography must be supplanted with electron-beam lithography as resolution requirements rise.

Electron pattern-producing systems can be divided into two categories; the first type exposes an electron-sensitive resist by scanning a single small electron beam in a defined pattern, the scanning electron microscope (SEM); and the second produces an entire pattern as one complete image (the projection exposure system). The slit-lens system developed under this contract is of the second type, i.e., a projection system. It is capable of producing high resolution patterns for surface acoustic wave transducers by transforming a pattern specified by a simple set of object mask holes into a set of very fine interdigitated lines. If a substrate coated with a positive electron-sensitive resist is exposed in this manner and then immersed in a suitable developer, the exposed areas (lines) constituting the images in the resist are developed away. Aluminum can then be deposited on the image areas and on the unremoved resist, which functions as a deposition mask, and the latter can be stripped away to leave a set of aluminum fingers bonded to the substrate in exact duplication of the electron exposure pattern. If such patterns are formed on a piezoelectric substrate (e.g., lithium niobate) and contact pads to each set of fingers are provided, then these fingers

become a microwave acoustic transducer, and pairs of these transducers suitably located on the same substrate function as delay lines.

The slit-lens projection system we have developed offers several advantages over the scanning type system for the routine production of such acoustic wave transducers; namely, the slit-lens system is simpler, and therefore less costly; it has a greater depth of field; and it should provide shorter exposure time than digitally controlled SEMs.

During this contract we designed and built a slit-lens exposure system and used it to produce successfully a range of interdigitated transducers and delay lines. In particular, we fabricated transducers having interfinger spacings of 2.3, 1.5, and 0.68 μ on lithium niobate, and these devices were shown to operate at 0.725, 1.15, and 2.8 GHz, respectively. These transducers were about 280 μ in transverse length (perpendicular to the propagation direction of the acoustic wave). The line width of the highest frequency transducer was approximately 3400 Å, and, judging from the definition of the edge of the fingers, this technique should be capable of fabricating transducers of even smaller dimensions and hence be useful for higher frequencies. Moreover, the technology can be extended readily to more complex structures, e.g., those having predesigned variations of finger widths and spacings in any given pattern.

I INTRODUCTION

During the past four years, considerable research and development work has been carried out on surface acoustic waves propagating in the VHF and UHF ranges in single-crystal piezoelectric materials. A piezoelectric material ensures that the surface acoustic wave carries along an associated electric field enabling the wave to be readily sampled or tapped at any point along its propagation path. The presence of this electric field has allowed a wide range of functional components to be realized, both for frequency filtering and, more significantly, time domain signal processing. The key to these realizations has been the metal-electrode interdigital transducer[1]* (see Figure 1) modified for specific applications by techniques such as grading the periodicity, grading the electrode overlap distance, and forming linear arrays of spatially separated wide-band transducers.

In spite of the great utility of the interdigital transducer, it has not been used often at frequencies above about 1 GHz, mainly because of the difficulty in fabricating transducers suitable for such high frequencies. Photolithographic techniques are generally capable of producing transducers with finger widths of about 1 μ and interfinger spacings of 2 μ. Structures with these dimensions on lithium niobate constitute transducers that operate at about 750 MHz.

The region of higher frequency devices has been exploited only with electron-beam exposure techniques that use electrons of effective wavelengths much smaller than the wavelengths available with light, even at

---

* Superscripts denote references listed at the end of the report.

1
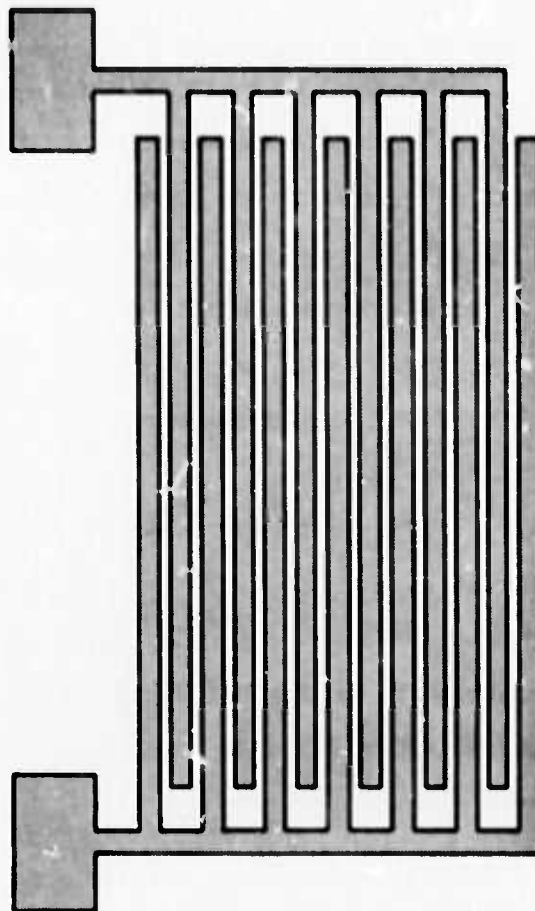
TA 651983 27

FIGURE 1   INTERDIGITAL SURFACE-ACOUSTIC-
WAVE TRANSDUCER

ultraviolet frequencies. The use of such small wavelengths greatly
enhances the resolution capabilities, and the scanning electron micro-
scope (SEM) has been used directly to produce transducers operating
at frequencies as high as 2.55 GHz[2,3,4] and indirectly to produce ultra-
high resolution masks for optical[5] and X-ray[6] lithography.

In general, although the SEM is a very versatile instrument having
well-documented capabilities for the microfabrication of microwave
acoustical transducers, it is also a very complex and expensive instrument.

2

The research carried out at Stanford Research Institute under this contract was aimed at demonstrating that a new electron-optical projection principle, called the "slit-lens" technique, is capable of producing acoustic microwave transducers with an apparatus that can be sufficiently simple and inexpensive to permit the dedication of such apparatus to this sole purpose. This new principle, described in the next section, makes use of the basic symmetries of typical transducer patterns and provides simple and stable exposures (on electron-sensitive resist) of an entire pattern in parallel rather than serially, as with the SEM. Thus, the loss of some of the versatility inherent in scanning systems is more than compensated for by the relative simplicity of the resulting exposure system.

II THE SLIT-LENS ELECTRON-BEAM EXPOSURE SYSTEM

The heart of the exposure system is a one-dimensional aperture lens produced by applying an accelerating electrostatic field between a slit-like aperture and a conducting substrate beneath it. Figure 2 shows a cross section of such a configuration, with the long dimension of the slit perpendicular to the page. At an appropriate field value the electrons from a distant source are focused by this slit-lens onto the substrate. By using slit-to-substrate spacings that are substantially smaller than the spacing between the object and the slit, the system can be used to provide one-dimensional images at very high
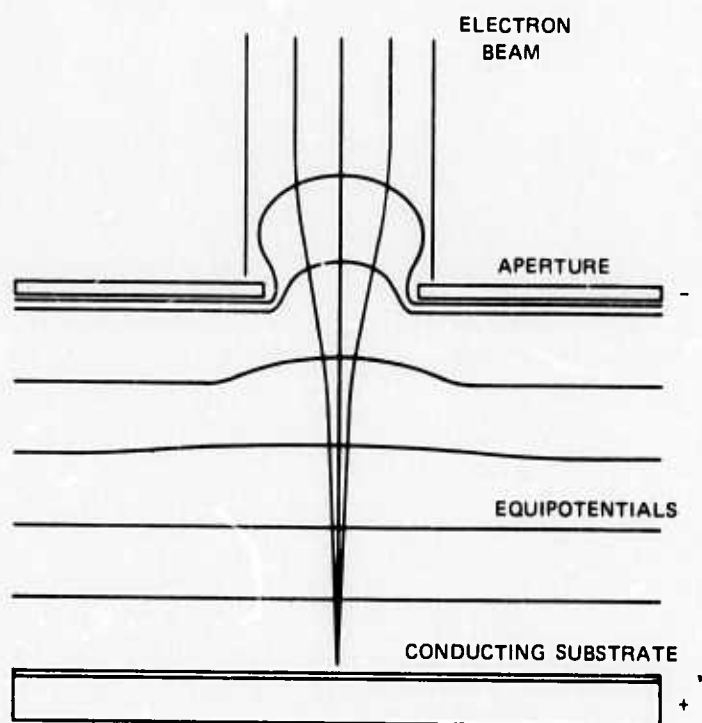
TA-651583-31R

FIGURE 2   APERTURE LENS ACTION

5

demagnifications. With this technique it is possible to use object mask patterns that are large enough to be made by standard photolithographic procedures and to produce electron-beam patterns several hundred times smaller.

A simplified illustration of the operation of the slit-lens is shown in Figure 3. Here, four round holes etched in a transmission mask act as object patterns when illuminated by a beam of electrons.

Each of these holes is demagnified in one dimension by the slit-lens so that a corresponding set of lines is produced on the substrate. The object pattern holes of diameter D and center-to-center interhole spacing L is transformed into a group of lines having widths MD and interline spacings of ML. The magnification factor M(< 1) can be approximated from first-order theory (see the Appendix) with the expression:

$$\frac{1}{M} = \frac{z_o \phi_s}{2\phi_o d} - 1 \quad ,$$ (1)

where

$z_o \equiv$ distance from object to lens

$d \equiv$ distance from lens to substrate

$\phi_s \equiv$ potential applied to substrate

$\phi_o \equiv$ potential applied to cathode (energy of electrons at object mask).

The ratio of voltages necessary to obtain focus for the slit-lens can also be worked out from first-order theory to give:

$$\frac{\phi_s}{\phi_o} = \frac{3}{2} + \frac{2d}{z_o} + \sqrt{\frac{9}{4} + \frac{2d}{z_o}}$$ (2)

ILLUMINATING
BEAM

d

MASK
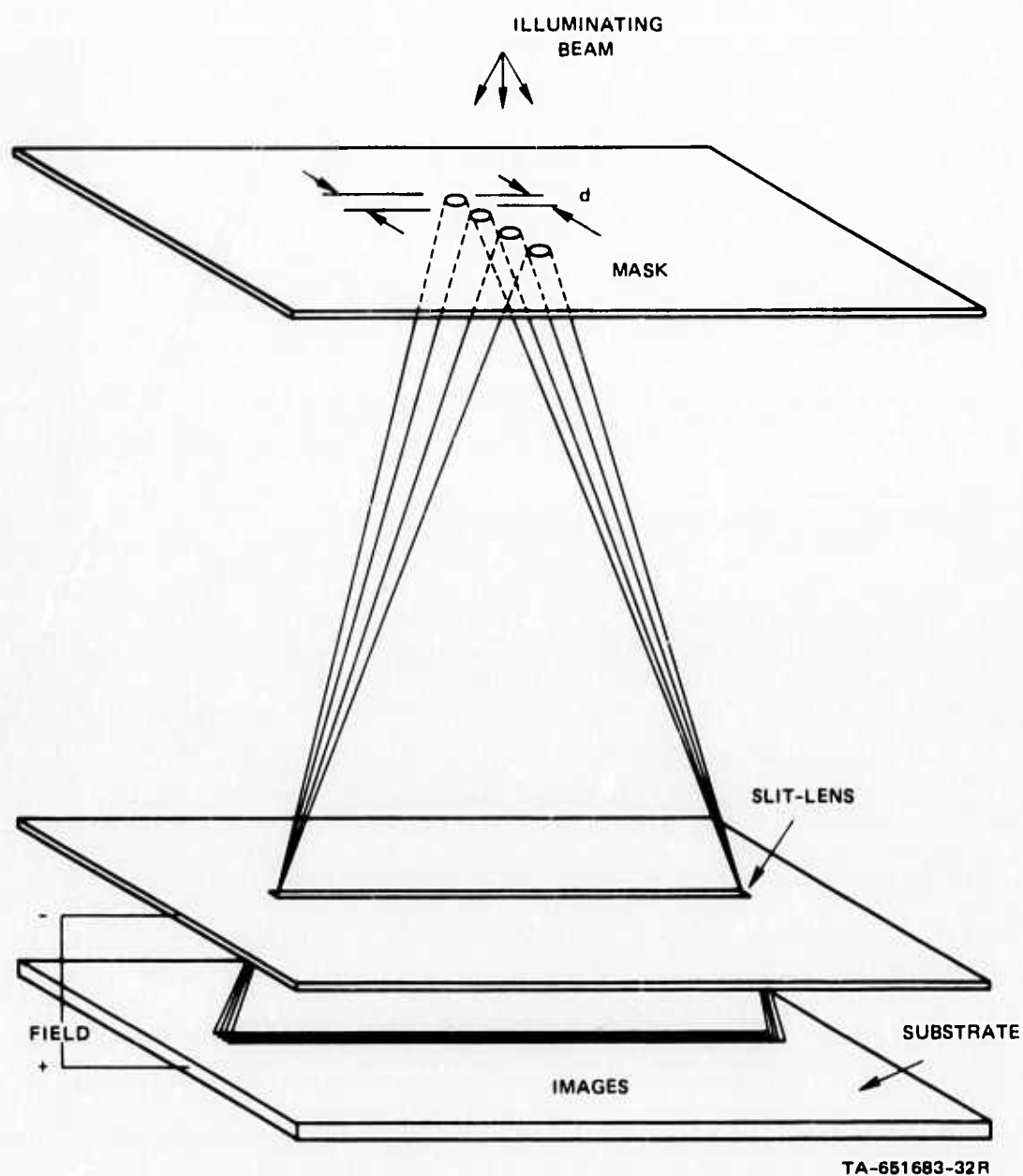
SLIT-LENS

FIELD

SUBSTRATE

IMAGES

TA-651683-32R

FIGURE 3   BASIC SLIT-LENS EXPOSURE SYSTEM

which, in the limit of small d/z_o (i.e., large demagnifications) works out to be

$$\frac{\Psi_s}{\Psi_o} = 3 \ .$$ (3)

Under the same condition Eq. (1) simplifies to:

$$\frac{1}{M} = \frac{3}{2} \ \frac{z_o}{d} \ ,$$ (4)

There are several advantages in using an aperture lens like the slit-lens in an electron-beam projection system. First of all, it is a very simple electrostatic lens. The entire lens consists of a single slit with an aperture placed directly above it. Construction of the lens is easily accomplished by well-known honing procedures. Alignment is automatically taken care of by properly placing the aperture over the slit, whereas in most other lenses, e.g., the Einzel lens, a number of electrodes must be precisely aligned with respect to one another for maximum resolution.

Another feature of the slit lens is its self-focusing capability. First-order theory shows that at high demagnification the image will always be in focus at the substrate plane regardless of the spacing between the slit and substrate. Hence it is possible to vary the demagnification over a large range and still keep the image in focus. Interpreted in another manner it can be stated that this sytem has exceptional depth of focus. First-order calculations disclose that the effective depth of field is increased by a factor of about 3/4 1/M over conventional electron-optical systems; e.g., for systems where the demagnification is 100 times, the depth of field is 75 times better than that for normal lenses. A displacement of 0.81 mm of the substrate is necessary to produce 0.1-μ defocus in the image plane. This feature
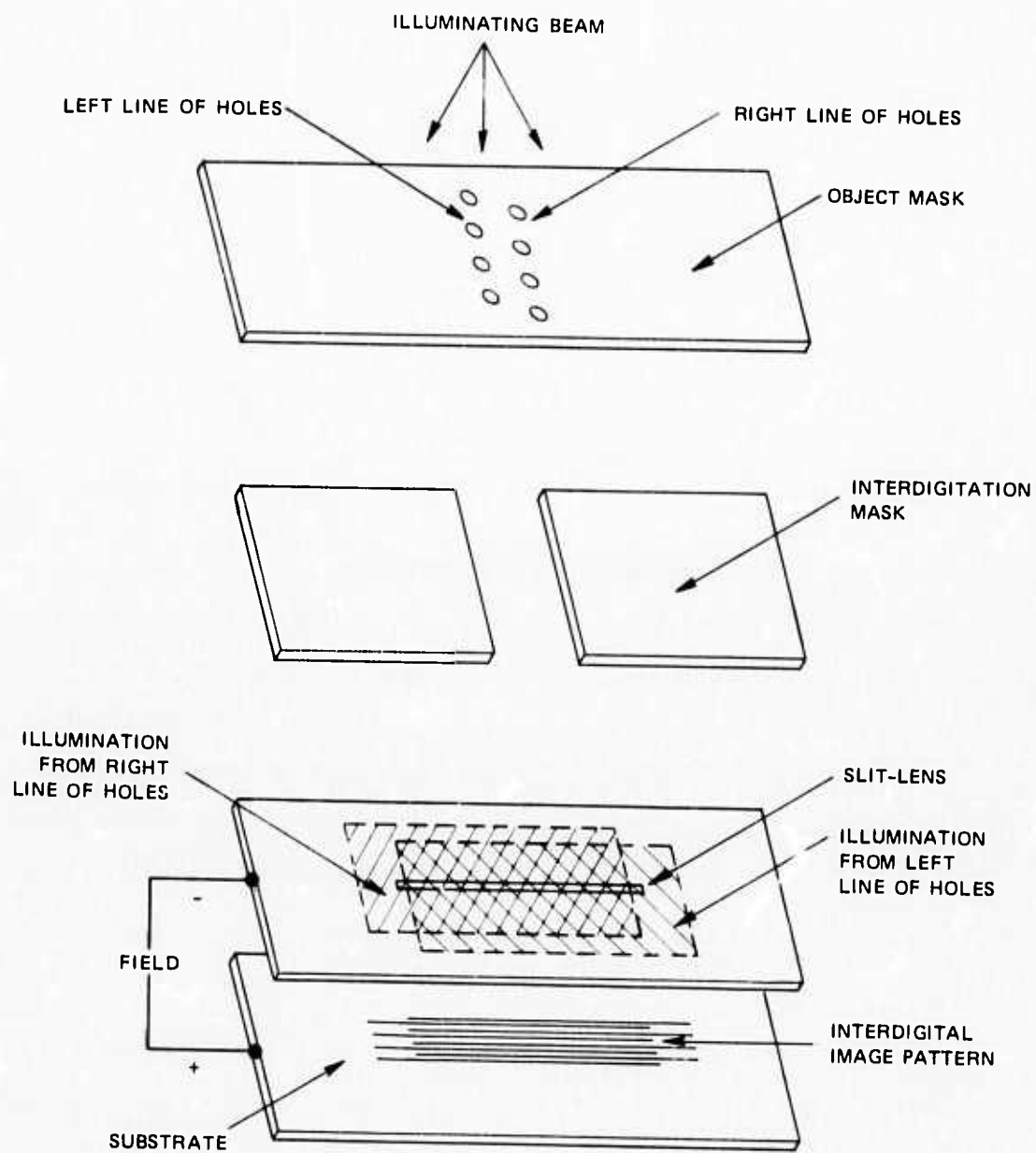
8

makes the lens system exceptionally tolerant to substrate uneveness, which limits the resolution of other projection and contact exposure systems. It also greatly facilitates pattern production by allowing small magnification changes to be brought about without refocusing.

Aperture lenses possess still another interesting feature. The ultimate resolution of an electron-optical lens system is determined mainly by the spherical aberration of the system. Point-source electrons that pass near the periphery of the lens are strongly deflected to cross the axis nearer the lens than those electrons that pass through the center of the lens. This defect is called spherical aberration and the increase in spot size is given by:

$$\zeta = C_3 \gamma^3 + C_5 \gamma^5 + \ldots \quad , \tag{5}$$

where γ is the semiangle of lens illumination and C_3 and C_5 are the third- and fifth-order spherical aberration coefficients, respectively. Ray tracing on the SRI computer has shown that, for two-dimensional aperture lenses (holes), the coefficients C_3 and C_5 have opposite signs. Thus, when the angle γ gets large enough, the spherical aberration is partially canceled out. This allows such a lens to be used at wider apertures than is normally possible. Although these computations have not been extended to the one-dimensional case of the slit-lens, the electron-optical characteristics should be similar.

Interdigitated lines can be produced by using an object mask having holes that are alternately laterally staggered and by interposing an interdigitation slit mask between the object mask and the slit-lens, as illustrated in Figure 4. The interdigitation mask is oriented perpendicularly to the slit-lens opening, so that when the slit-lens is illuminated from the object pattern, the interdigitation mask offsets the set of images produced by the slit-lens from each row of holes. The

9

ILLUMINATING BEAM

LEFT LINE OF HOLES

RIGHT LINE OF HOLES

OBJECT MASK

INTERDIGITATION
MASK

ILLUMINATION
FROM RIGHT
LINE OF HOLES

SLIT-LENS

ILLUMINATION
FROM LEFT
LINE OF HOLES

FIELD

INTERDIGITAL
IMAGE PATTERN

SUBSTRATE

SA-1909-1

FIGURE 4   ARRANGEMENT FOR PRODUCING INTERDIGITAL PATTERNS

10

vertical position and slit spacing of the interdigitation mask can be readily varied to produce transducers of various active areas and connecting finger lengths.

A simplified view of the slit-lens exposure system is shown in Figure 5. The system is comprised of two assemblies with a drift space between them. The electron-gun and object mask assembly is situated at the bottom of the system and the slit-lens and substrate holder are at the top. This arrangement gives maximum accessibility to the substrate through the top of the vacuum column (not shown). The base of the column is pumped with a liquid nitrogen-trapped, 6-inch diffusion pump.

To illuminate the slit-lens properly, each hole in the object mask must be evenly illuminated. Uniform exposures at the substrate require not only that the intensity of the object mask be even, but also that the angular distribution of the emerging electrons be isotropic. Illumination of the object mask with a broad area cathode would provide a suitable solution to the uniformity problem. However, broad area cathodes of either the barium oxide type or the dispenser type do not have long lives in demountable vacuum systems, whereas tungsten filament emitters do. Therefore, this problem was surmounted by using a single long tungsten wire as the emitter in a triode gun structure and providing a set of deflection plates to scan the emerging ribbon beam of electrons transversely to yield the equivalent effect of a large area cathode. Specifically, as shown in Figure 5, the grid and anode plates are formed of slits to produce a gun that is a one-dimensional analog of the standard electron microscope gun configuration. The beam of electrons that emerges from the gun is spatially defined by an aperture and then passes through a double-deflection system. A 50-Hz triangle voltage is applied to the first set of deflector plates so
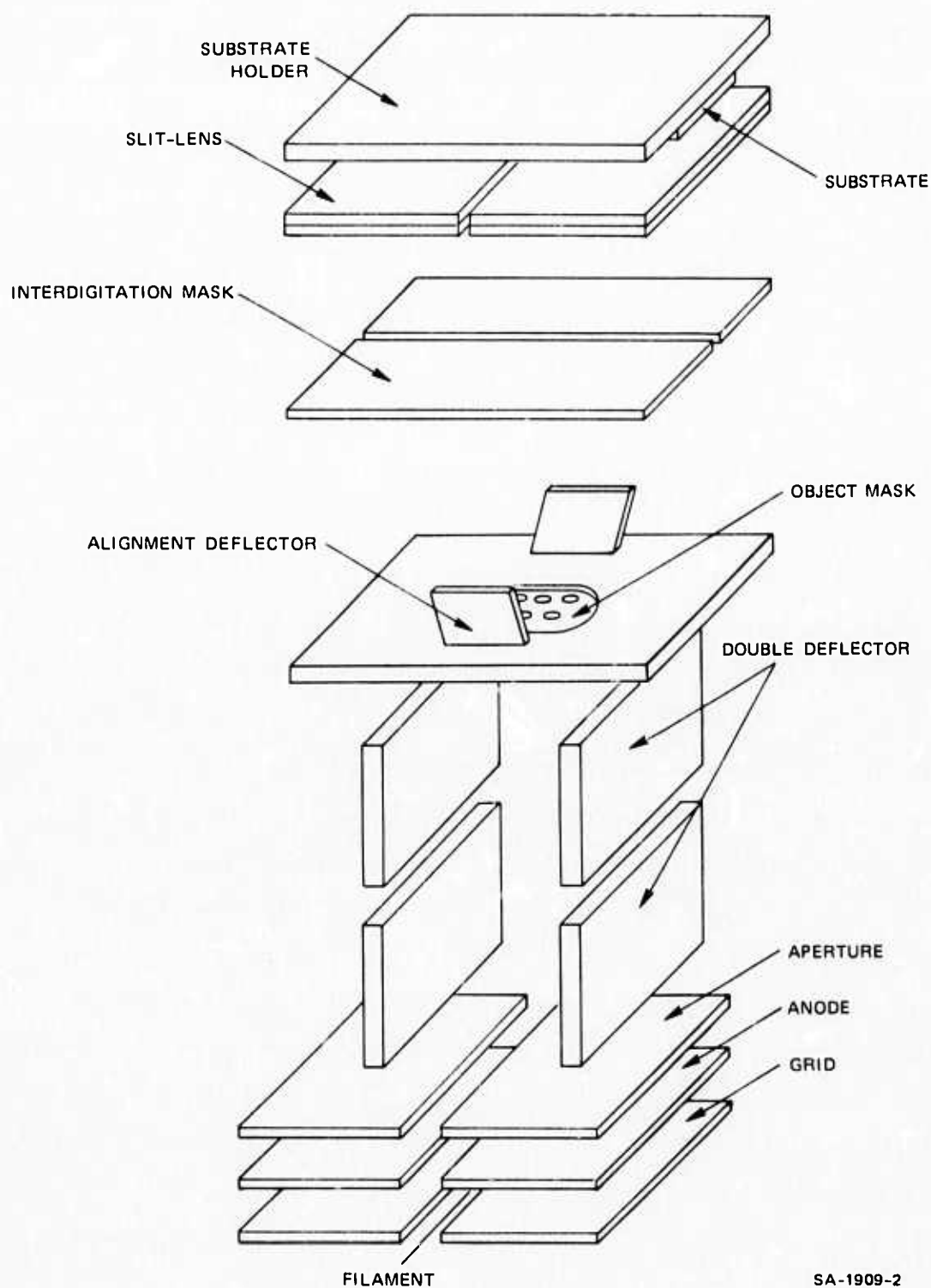
11

FIGURE 5 SLIT-LENS EXPOSURE SYSTEM

SA-1909-2

that the beam of electrons is uniformly swept through a range of angles. By applying a portion of this triangle wave to the second set of deflectors, the beam is brought back on axis in the plane of the object mask to maintain continuous illumination during scanning, thereby yielding the equivalent of the illumination from a broad area cathode of low current density. The low current density is of no consequence, however, because exposure times with this scanning illumination technique are quite acceptable.

Although we are using scanning as a means of obtaining uniform exposure, this system should not be confused with the scanning electron microscope. In the latter instrument the actual position of the electron beam is controlled by precise scanning voltages. However, in the slit-lens system the scanning is done before the beam reaches an object mask and hence can be thought of as a scanning condenser lens. In this function only a simple unregulated triangle wave is needed for operation.

A postobject mask deflector is used to align the beam laterally on the interdigitation mask. The dc voltage applied to this deflector serves to cancel out the effects of small misalignments and residual magnetic fields within the drift space.

The upper slit-lens assembly consists of the interdigitation mask, the slit-lens with its built-in aperture, and the substrate holder. In the simplest construction all the slit-lens parts are made of movable molybdenum sheets that have smooth straight edges. The slit width can be varied over a large range. The sample holder is constructed with a guard electrode surrounding the sample so that the plane-parallel field between the substrate and the slit-lens electrode is not perturbed by the edges of the substrate.

The structure of the exposure system is supported within a self-aligning cylindrical vacuum jacket. The entire system is depicted in Figure 6, and Figure 7 shows the disassembled column. Each section has a vacuum seal, which is secured by the weight of the column and the atmospheric pressure differential when the column is under vacuum. Since no section of the column is more than 7 inches long, each section is relatively light, and these parts can be readily manipulated by hand. The column can be completely unstacked in a matter of minutes.

A soft steel is used in the construction of the vacuum jacket to aid in the electromagnetic shielding within the column. Two concentric 0.010-inch-thick, permalloy internal shields are used to reduce further low frequency magnetic disturbances in the critical drift region.

Typical dimensions and operating parameters for the system used in this work are given in Table 1.

Table 1	
TYPICAL EXPOSURE PARAMETERS	
Interdigitation slit opening	0.012 inch
Slit-lens aperture opening	0.005 inch
Slit-lens electrode opening	0.020 inch
Substrate holder voltage	5000 V
Filament voltage	$\sim$ 1500 V
Grid voltage	- 15 V
Cathode current	$\sim$ 6 mA

Sample current is measured at the slit-lens aperture, which is grounded through an external nanoammeter. This current is used to establish the exposure time. Exposure is terminated by changing the sample voltage from +5000 V to cathode potential. This form of
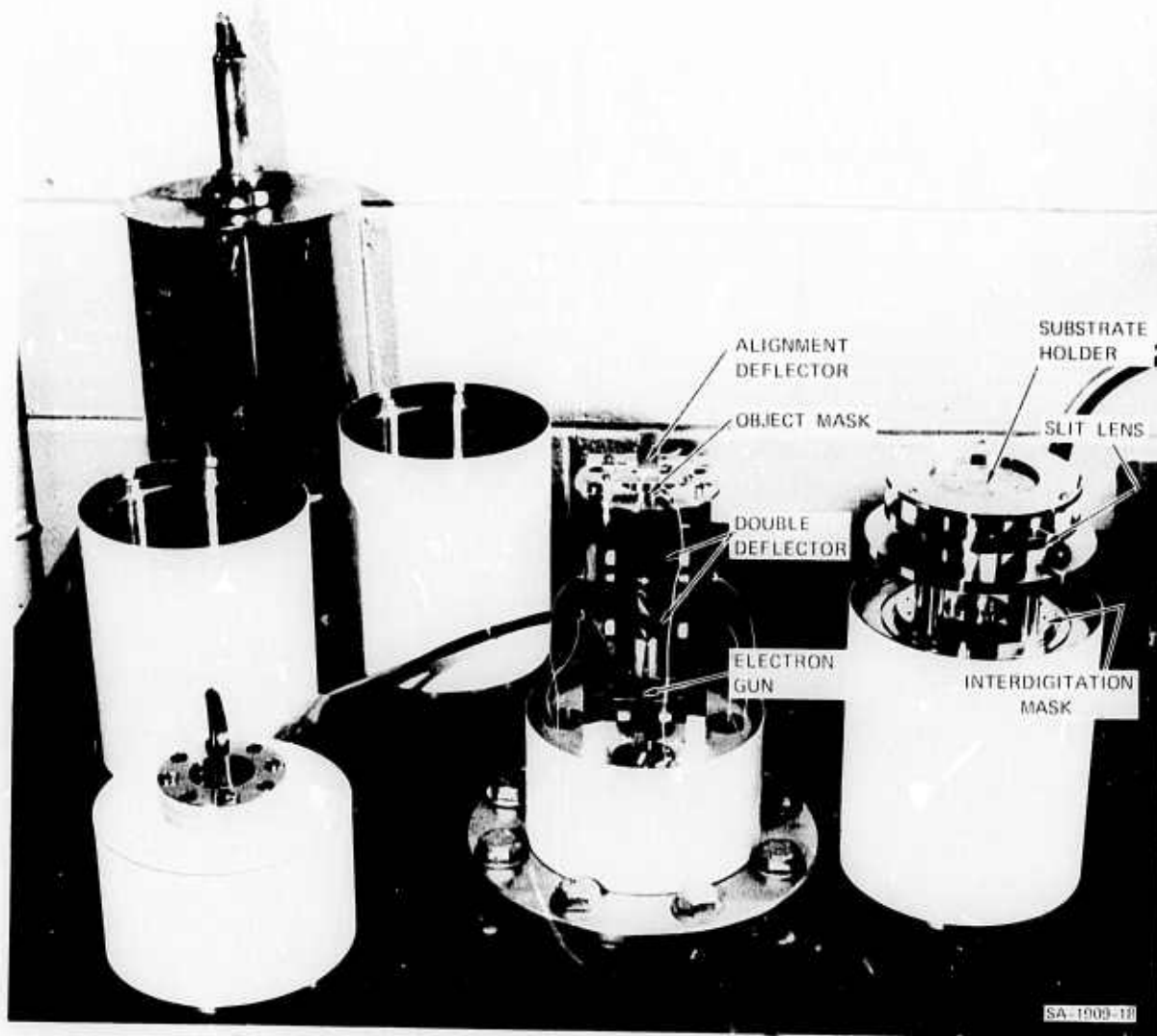
14

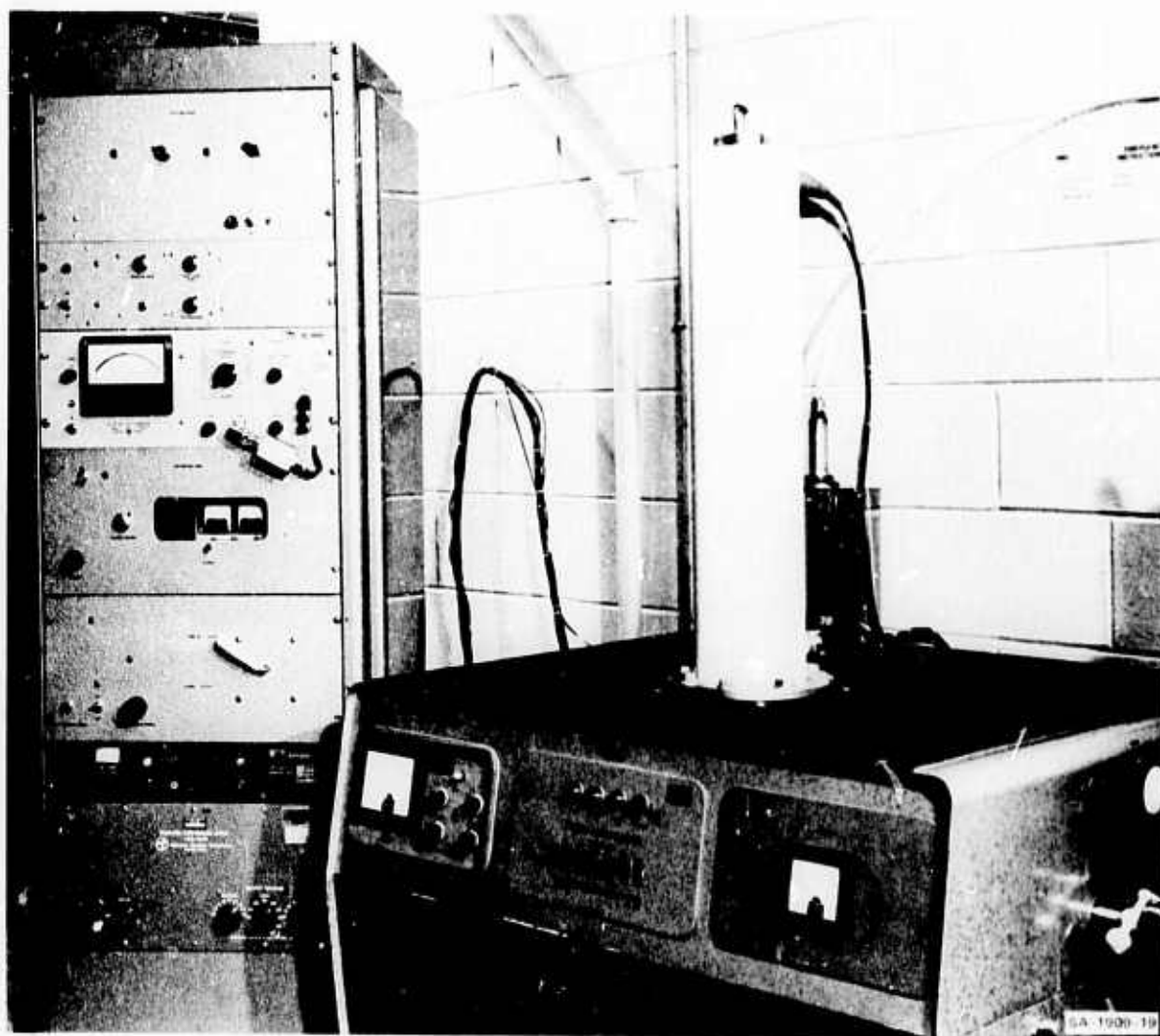FIGURE 6   COMPONENTS OF THE SLIT-LENS SYSTEM

FIGURE 7   ASSEMBLED SLIT-LENS SYSTEM

electrostatic shuttering allows the low voltage beam to stabilize in
the column so that only the last fraction of an inch of beam travel
is affected by the shutter mechanism.

The volume of the column has been kept to a minimum to provide fast
evacuation rates. Typically, a vacuum of 8×10^{-6} torr can be obtained
in about 3 minutes from the time that the roughing cycle is initiated.

A simple gravity vacuum seal on the top of the column makes removal
and insertion of samples a facile operation and, once the column has
been properly set up and aligned, exposures can be produced reliably in
a routine manner.

The usual delay-line structure consists of two interdigital trans-
ducers spaced and oriented appropriately on a piezoelectric substrate.
Exposure times on the resist material (polymethyl methacrylate) range
from 10 s to about 1 minute per transducer, depending on transducer
size. However, exposure times can be easily reduced below these
figures if this proves desirable. Typical turnaround times between
successive pumpdown exposure operations can be as short as 10 minutes.
At present, transducer pairs are made one transducer at a time by moving
the substrate between exposures (step and repeat). However, it is
feasible to upgrade the present system to produce transducer pairs (i.e.,
the pattern required for a delay line) in a single exposure.

17

III THIN-FILM PROCESSES FOR TRANSDUCER FABRICATION

Before pattern exposure, the lithium niobate substrate is given a thorough chemical cleaning, followed by an air plasma etch to ensure a contamination-free surface. Polymethyl(methacrylate) (PMM) is used as the positive electron-sensitive resist and is applied with a commercial resist spinner and then baked to attain maximum adhesion. Final resist thickness is in the range of 1000 to 1100 Å. The resist is then over-coated with a conducting film that acts as an electrostatic shield during exposure to prevent charges buried in the insulating resist from deflecting the electron beam. We have used both aluminum and con-ducting polymer films, 500 to 700 Å thick, for this shield layer. The conducting polymer film offers the advantage that it dissolves away during the development process, whereas the aluminum film must be etched off in orthophosphoric acid before development of the resist. The shielding capability of the aluminum, however, is somewhat greater, so that the appropriate shield layer is dependent on the thickness of the resist, beam current, and exposure time.

Figure 8(a) is a cross-sectional view of the PMM being exposed in a strip that will eventually become a transducer finger. Total charge density at the PMM surface needed for complete exposure is estimated to be from 50 to 70 microcoulombs/square centimeter. The shield layer is removed in the case of aluminum, and isopropyl alcohol is used to dissolve preferentially the exposed region, leaving the unexposed region of the resist with an overhanging lip. This undercut [Figure 8(b)] is evident in the scanning electron micrograph, Figure 9, which depicts a cross-sectional view of the substrate/resist sandwich.

19

ELECTRON BEAM

ANTICHARGING LAYER
(ALUMINUM OR CONDUCTING
POLYMER)

500 Å

1100 Å

RESIST

SUBSTRATE

EXPOSURE

DEVELOPMENT UNDERCUT

RESIST

DEVELOPMENT

ALUMINUM

950 Å

RESIST

DEPOSITION

ALUMINUM TRANSDUCER PATTERN

950 Å

STRIP OPERATION
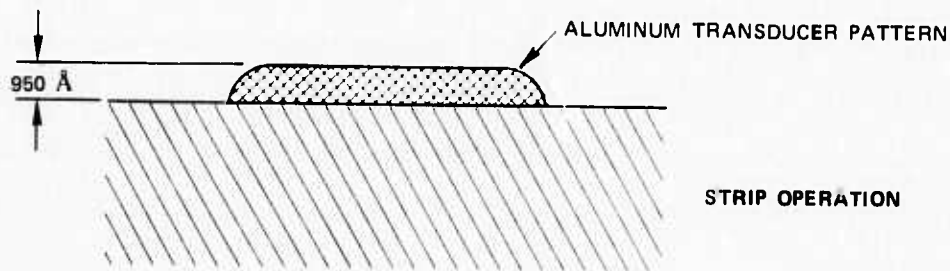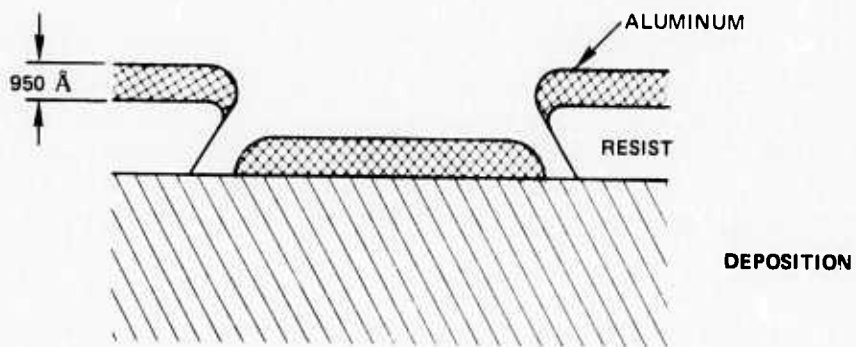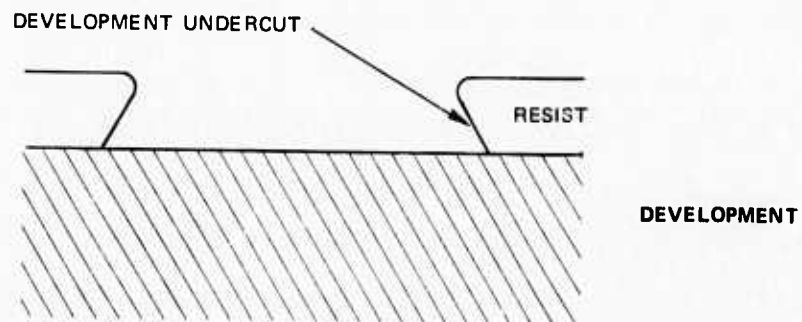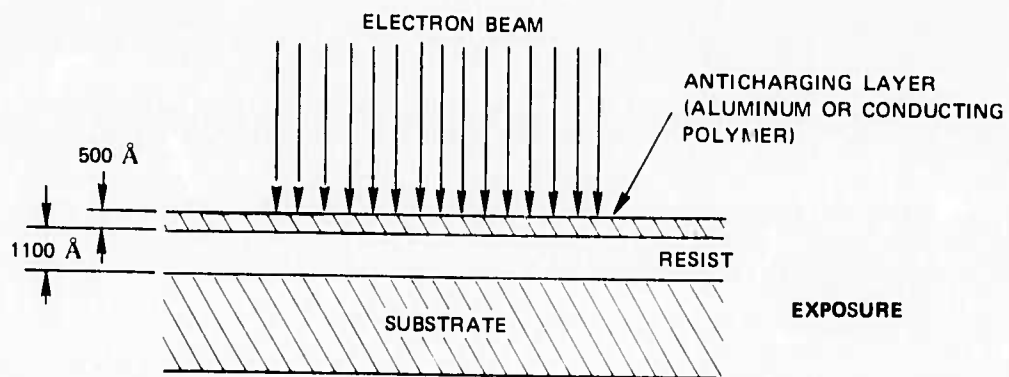
SA-1909-3

FIGURE 8   TRANSDUCER FINGER FABRICATION

20

FIGURE 9   CROSS-SECTION OF ALUMINUM FILM
OVER DEVELOPED RESIST

A gentle treatment in air glow discharge cleans the residue from the surface, and approximately 950 Å of aluminum is electron-beam evaporated onto the surface to form the structure depicted in Figure 8(c). The undercut of the resist produces a physical separation between the aluminum on top of the resist and the aluminum forming the actual transducer fingers, and a gentle ultrasonification of the substrate in hot trichlorethylene removes the resist and the aluminum adhering to it. This "lift-off" procedure leaves fingers of aluminum on the piezo-electric substrate in the same pattern as the electron beam image [Figure 8(d)].

21

The pads on the end of the transducers are made by a similar
"lift-off" technique. A positive photoresist, GAF Microline, is exposed
with the light image of the desired pad pattern and developed in GAF
developer to remove the resist in the exposed pad areas. Aluminum is
now evaporated onto the substrate using the unexposed resist as a mask.
Removal of the resist in hot acetone also removes the aluminum overlying
the resist, leaving behind aluminum bonding pads at the ends of the
interdigitated lines.

IV MICROFABRICATION RESULTS

Early in the program a simplified slit-lens exposure apparatus was constructed with a view toward exploring the capabilities of such a system. This system was assembled from components of other electron-beam screen lens apparatus, and simple stainless steel razor blades were used as a slit-lens. Simple, noninterdigitated, three-line patterns were generated by this apparatus which primarily served to point out problem areas, to determine operating parameters, and to define the edge resolution of the process.

Figure 10 is a scanning electron micrograph showing a portion of such a pattern of three aluminum lines on a silicon substrate. The
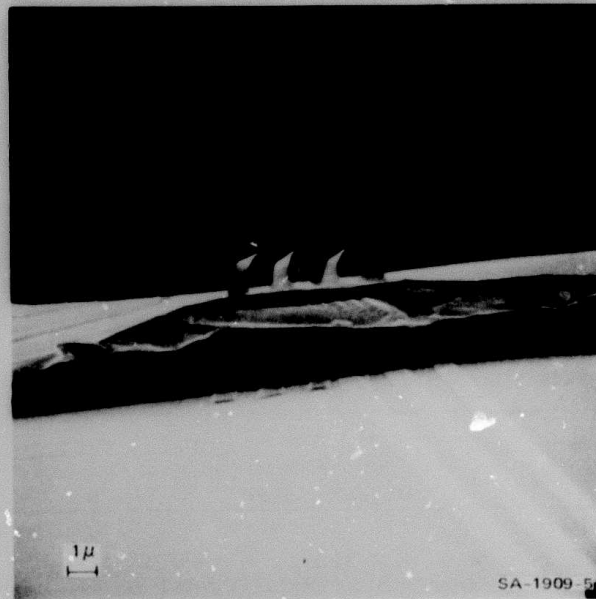

1μ

SA-1909-5

FIGURE 10   ONE MICRON WIDE ALUMINUM
LINES ON SILICON

23

lines are spaced approximately on 2-μ centers, and the width of the lines is about 1 μ. The lines extend for 1 cm across the surface of the silicon. By a fortunate circumstance a portion of the silicon at the substrate's edge became chipped and the resulting flake flipped over while it was being held tenaciously by the three aluminum micro-tentacles. This stroke of luck affords a good view of the uniformity of the aluminum lines and shows that the edge resolution is very high.

With the impetus of these initial results, the improved instrument described in the previous section was designed and built. On completion of the construction and debugging of this instrument, transducers of three different sizes were fabricated on y-cut, z-propagating lithium niobate substrates to form operational delay lines. Table 2 summarizes the dimensions of these transducers and the corresponding slit-lens sytem parameters. The first devices consisted of sets of transducers with interfinger spacings of 2.3 μ and finger widths of 1.3 μ (Type 1 of Table 2). The production of these devices was used to tune up the exposure apparatus for best definition and to aid in the development of ancillary thin-film fabrication techniques.

Table 2

MEASURED SLIT-LENS CHARACTERISTICS

Transducer Type	Interfinger Spacing (μ)	Spacing (μ) Between Object Holes	Focus Voltage Ratio Φ_s/Φ_o	Demagni-fication
1	2.33 ± 0.02	152	3.33 ± 0.01	65 ± 2 ×
2	1.50 ± 0.02	152	3.47 ± 0.01	102 ± 3 ×
3	0.68 ± 0.02	152	3.88 ± 0.01	225 ± 6 ×

24

By changing the spacing between the slit-lens and the substrate, the demagnification of the same object pattern was increased to produce $0.75-\mu$ lines on $1.50-\mu$ centers (Type 2). Finally, the demagnification was increased to over 200 times and patterns with 6800 $\overset{\circ}{A}$ spacing and 3400 $\overset{\circ}{A}$ lines were made (Type 3). Each of these transducers was fabricated with 10 interdigitated fingers with an active transducer length of about 280 μ.

Table 3 summarizes the first-order properties of the slit-lens as deduced from the parameters in Table 2. Here it can be noted that

Table 3			
FIRST-ORDER CALCULATED SLIT-LENS CHARACTERISTICS			
Transducer Type	Sample Spacing d (inch)	Demagni- fication 1/M	Focus Voltage Ratio ϕ_s/ϕ_o
1	0.357	66.7 $\times$	3.07
2	0.232	108 $\times$	3.04
3	0.107	263 $\times$	3.03

first-order theory approximately describes the operation of the system. However, it is in error by about 6 percent and 16 percent, respectively, in the demagnifications for transducer Types 2 and 3. Moreover, the errors in focus ratio ϕ_s/ϕ_o range from 10 percent to 28 percent. Thus, although the basic properties of the slit-lens can be obtained by the simplified model, more accurate theory must be developed to obtain closer predictions. This is especially true in the limit of small f-number lenses, i.e., for large slit widths or small slit-lens-to-substrate spacings.

Figure 11 shows a completed Type 1 transducer on lithium niobate after the pads have been added for bonding. Most substrates were processed to provide four transducers of identical patterns having an intertransducer spacing of 0.200 inch.
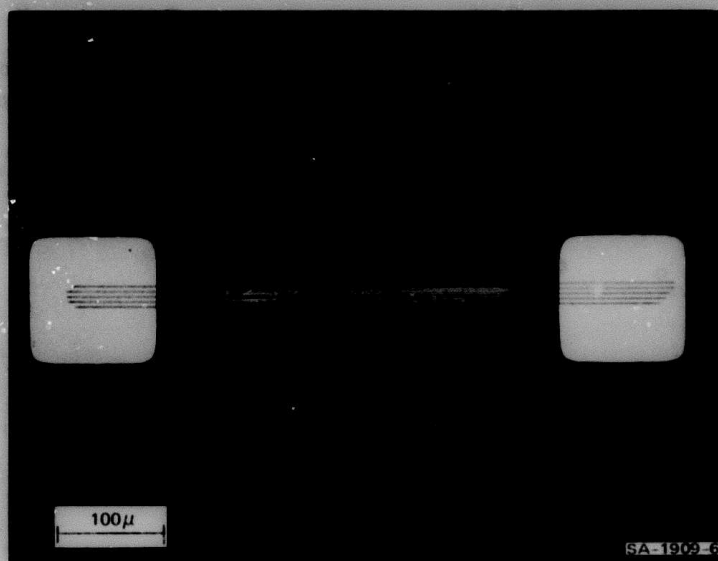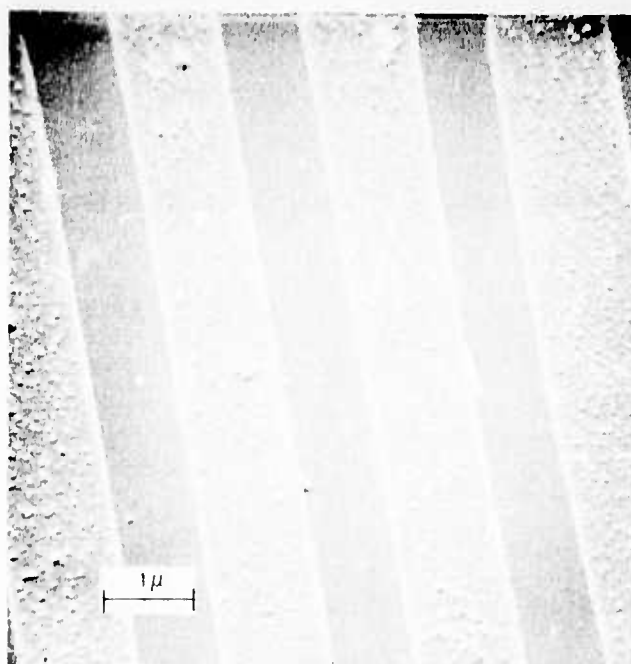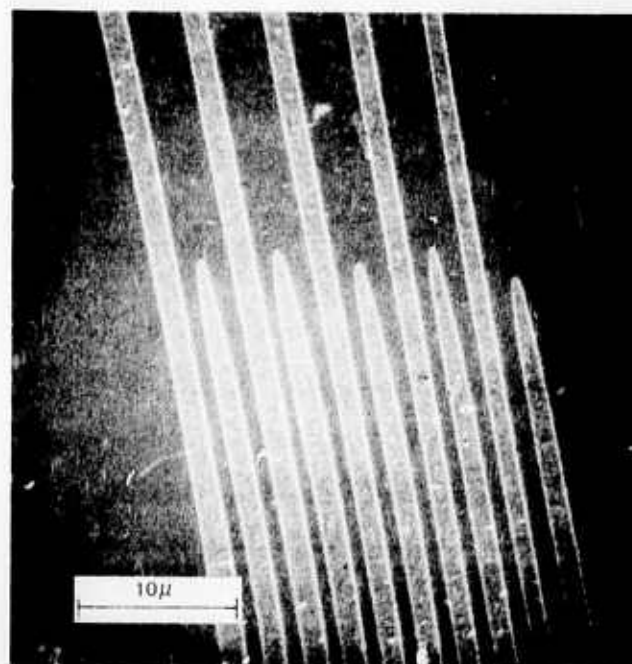

FIGURE 11   INTERDIGITATED TRANSDUCER ON
             LITHIUM NIOBATE—2.3μ FINGER
             SPACING

SA-1909-7

FIGURE 12   ALUMINUM TRANSDUCER FINGER—2.3μ SPACING

Figure 12 shows the fingers of a similar Type-1 transducer at two different magnifications. The first of the scanning electron micrographs shows one of the ends of the interdigitation region of the fingers. It can be seen that the ends of the fingers are not perfectly square or precisely the same length. The reason for these small departures is that the slit-lens demagnifies only in the direction perpendicular to the fingers. In forming the image corresponding to the ends of the fingers, the interdigitation slit acts as a shadow mask and, because of the finite size of the object hole, a penumbra that extends for about 10 μ is formed at the finger ends. Small illumination variations from hole to hole on the object mask cause intensity variations on the corresponding penumbra regions and hence in the exposure dosages, thereby introducing variations in effective line length. The magnitude of this effect is quite tolerable, however, as can be seen in Figure 12 where the variance in finger length is less than ± 1.5 μ.

Another defect observable in these micrographs is that there are small variations in line width within the transducer. These result from the fact that uniformly illuminated round holes in the object mask do not transform into uniformly illuminated lines when projected by the slit-lens. In fact, the lines have a sinusoidal intensity distribution along their widths. Thus, small intensity variations from hole to hole are reflected as width variations in the final transducer lines.

This defect can be totally eliminated if square-shaped holes are used in the object mask. The slit-lens transforms square holes into uniformly illuminated lines, and this produces equal line widths regardless of local intensity variations at the object mask.

Figure 13 is a scanning electron micrograph of the aluminum fingers in the highest frequency transducer (Type 3). The line widths depicted here are about 3400 $\mathring{A}$. The high resolution of the fabrication process is very evident in this micrograph; edge resolution seems to be considerably less than 1000 $\mathring{A}$. On the basis of these results it appears that the limits of resolution have not yet been attained and that even higher frequency devices can be fabricated with this technique.
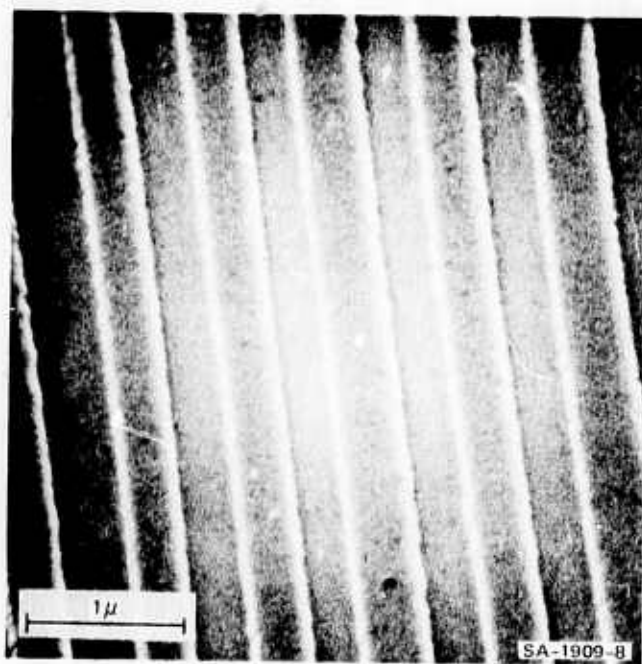

FIGURE 13   TRANSDUCER FINGERS—6800 Å SPACING

V OPERATIONAL CHARACTERISTICS OF HIGH FREQUENCY
SURFACE ACOUSTIC WAVE INTERDIGITAL TRANSDUCERS

A.   Measurement Techniques

The three types of high frequency interdigital transducers fabricated by the slit-lens system were evaluated by three measurement techniques: (1) measurement of the pulsed RF insertion loss between pairs of similar interdigital transducers on the same substrate, (2) measurement of the CW insertion loss between pairs of similar transducers, and (3) measurement of the electrical input impedance of a single transducer using a Hewlett-Packard automatic network analyzer. The pulsed and CW insertion loss measurements should yield similar results if the spurious electromagnetic feedthrough and bulk wave signals can be kept well below the main surface wave signal. The insertion loss measurements are of value in determining the quality of a complete surface wave delay line consisting of two transducers. However, this measurement is influenced by such effects as propagation attenuation, acoustic beam diffraction, and misalignment between the two surface wave transducers. On the other hand, the measurement of a transducer's one-port input impedance allows direct observation of the frequency-dependent coupling of that transducer to surface waves and can be used to determine the quality of the acoustic wave transducer if the associated parasitic circuit elements of the transducer are known. The pulsed insertion loss measurements were made using a standard heterodyne receiver system and substituting known attenuators in place of the surface wave delay line under test to obtain a given reference signal level. The CW insertion loss and input impedance measurements were made on a Hewlett-Packard automatic network analyzer. This instrument is capable of making accurate impedance and insertion loss measurements from 110 MHz to

31

12.4 GHz at frequency intervals as small as 2 MHz. Care was taken to establish the precise location of the reference plane for the impedance measurements to yield accurate device characterization. Care was also taken to minimize any stray electrical parasitics that might influence this measurement.

The interdigital surface acoustic wave transducer patterns were fabricated on YZ LiNbO$_3$ plates. The electrodes were aligned with the reference edge of the substrate so that the acoustic beam would propagate as colinearly with the crystalline z-axis as possible. The YZ LiNbO$_3$ material was selected because the electromechanical surface wave coupling is large, the propagation loss of surface waves is relatively low (loss $\approx$ 2.4 dB/cm at 1 GHz), and the surface waves have small diffraction loss for propagation in the z-direction. The dimension of the substrates were: 12.5 mm, 3mm, and 25 mm in the X,Y,Z crystal directions, respectively, with one Y face polished optically flat (to 1/10 wavelength of light) and scratch free under microscopic evaluation.

As detailed previously, the transducers were composed of 10 interdigital electrodes or 4-1/2 interdigital periods. This number is about the right number of periods $N = \pi/4k^2 \approx 4$ for YZ LiNbO$_3$ for optimum transducer bandwidth when operated under tuned and matched conditions. For untuned operation, the transducer bandwidth should be 1/N or 22 percent for this transducer design. The transducer acoustic aperture, or lateral width W, was measured to be 280 μm for all transducers fabricated.

B.   Microwave Acoustic Surface Wave Test Fixture

To measure accurately the performance of the high frequency interdigital transducers, a suitable microwave test fixture was necessary. The microstrip test fixture shown in Figure 14 was constructed to have four 50-Ω characteristic impedance transmission lines fabricated on

32
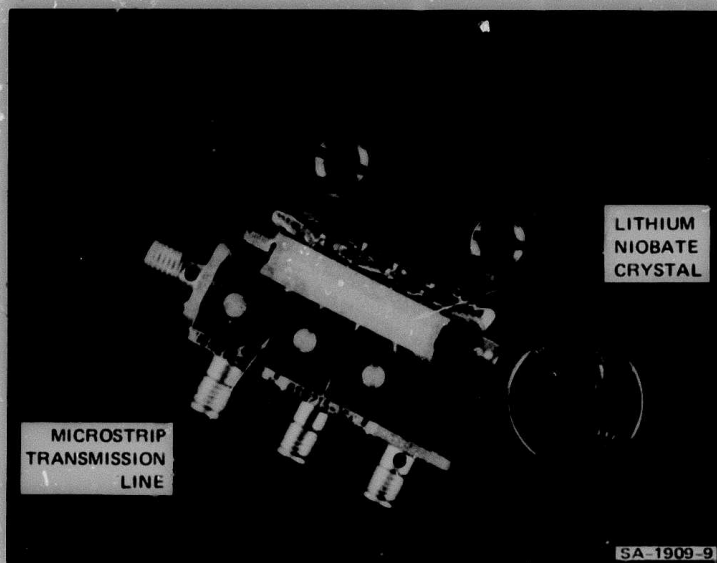
FIGURE 14   MICROSTRIP TEST FIXTURE USED TO EVALUATE
INTERDIGITAL SURFACE-WAVE TRANSDUCERS

copper-clad epoxy board (relative dielectric constant $\varepsilon_r = 4.9$). The
microstrip lines of 0.58-mm width were small enough to ensure low
electrical crosstalk between the various lines. Each line was attached
to a subminiature adapter output port to facilitate connection of the
test fixture to the measuring ports of the network analyzer. Elec-
trical connection to the transducer was accomplished by thermocompression
bonding 0.7-mil diameter gold bond wires between the ends of the micro-
strip lines and the interdigital transducer pads. As shown in Figure
14, a common ground return was provided on the opposite side of the
$LiNbO_3$ crystal. Unfortunately, the small transducer size requires long

33

bond wire connections, which in turn causes direct electromagnetic coupling between the closely spaced ($\approx$ 0.5=cm separation) transducers. Figures 15 and 18 (shown later) show this initial RF feedthrough signal from direct coupling. It was found that this spurious signal could be substantially reduced (by 20 to 30 dB) if a ground plane shield (not illustrated) was used to surround the transducers on the LiNbO$_3$ and the bond wires were kept as short as possible. A modified test fixture having this ground shield was used to make all CW insertion loss measurements on Types 1 and 2 delay lines (725 MHz and 1.15 GHz, respectively).

The test fixture shown in Figure 14 allows accurate determination of the length of transmission line between the connector and the transducer. This permits effective measurement of the reference plane and allows it to be set at the point where the bond wire attaches to the microstrip line. Because of the high Q of these surface wave transducers, precise reference plane location is necessary for accurate impedance determination.

Type 1 high frequency surface wave delay lines were fabricated with 4 identical transducer patterns on each substrate, with the transducers spaced 0.5 cm apart. Type 2 delay lines had 5 transducers spaced 0.32 cm apart. The spacing between transducers of 0.5 cm corresponds to a signal time delay of 1.46-μs on YZ LiNbO$_3$. This delay was long enough to allow resolution of the surface wave signal from the direct electromagnetic feedthrough signals. The transducers pads were $\approx$ 100 μm square, which provided enough area for easy wire bonding.

34

C.   Experimental Evaluation of Type 1 Transducer Patterns (2.3-μ Interfinger Spacing and 725-MHz Center Frequency).

Insertion loss and input impedance measurements were carried out on two surface wave delay lines, each having four interdigital transducer patterns. These patterns were fabricated to have a periodicity of 4.66 ± 0.04 μm. The patterns appear under microscopic evaluation to be of uniformly high quality and without shorted or broken electrodes. Figure 15 illustrates typical pulse delay characteristics of the surface wave device and the corresponding "untuned" insertion loss measurements made at 725 MHz. Figure 15(a) shows the short (0.5 μs) pulse of RF signal applied to an end transducer of the four. The resulting output signals from each of the other three transducers is seen in Figures 15(b), (c), and (d). The measured time delay τ between adjacent transducers of 1.45 μs agreed well with the expected time delay of 1.46 μs calculated from the formula:

$$\tau = \frac{\ell}{v_s} \quad (\mu s) \quad , \tag{6}$$

where ℓ is the distance between the transducers (equaling 0.508 cm in this case) and v_s is the surface wave velocity 3.488×10^5 cm/sec for YZ LiNbO$_3$.

The sources of delay line insertion loss in general can be attributed to three main causes:

(1)   Propagation loss--attenuation of the surface wave as it propagates between input and output transducers.

(2)   Loss due to the transducer geometry--or diffraction and beam steering due to acoustic anisotropy of the substrate material.

(3)   Transducer loss--namely, conduction loss within the metal electrodes, impedance mismatch between the transducer and the electrical circuit, and bulk wave excitation.

35

(a) INPUT TO
TRANSDUCER 1

(b) OUTPUT FROM
TRANSDUCER 2

INSERTION LOSS
= 23.5 dB

(c) OUTPUT FROM
TRANSDUCER 3

INSERTION LOSS
= 24.8 dB

(d) OUTPUT FROM
TRANSDUCER 4

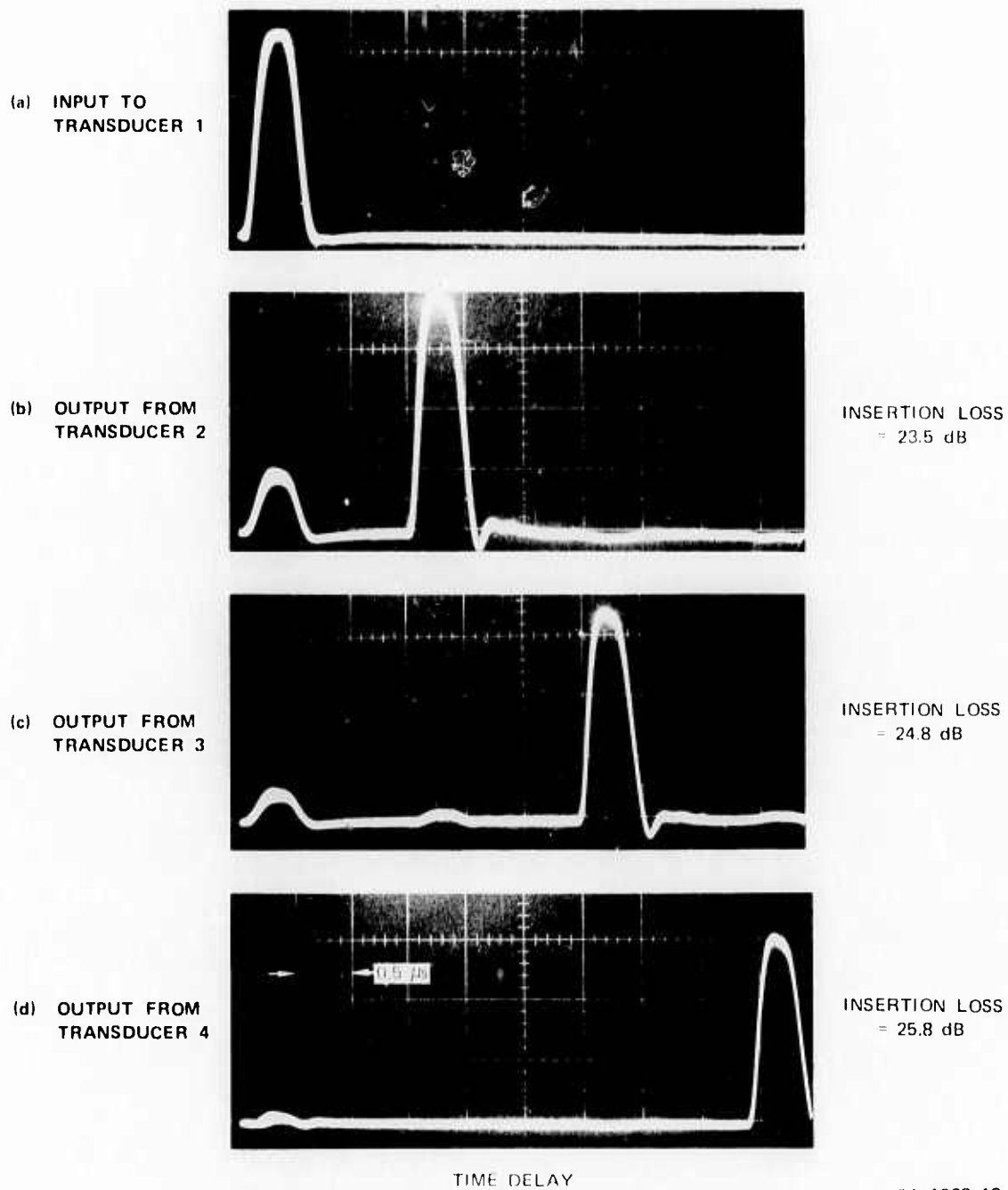INSERTION LOSS
= 25.8 dB

TIME DELAY

SA-1909-10

FIGURE 15   RF PULSE TRANSMISSION THROUGH TYPE 1 SURFACE-WAVE
DELAY LINE AT 725 MHz

The average difference in insertion loss measured between adjacent transducers spaced 1.45 μs apart was 1.16 dB. This yields an average loss per unit time of 0.80 dB/μs at 725 MHz.

Measurements of the propagation loss of surface waves on YZ LiNbO$_3$ have been carried out by Slobodnik[7] et al. and Lean[8] et al. in the frequency range 0.2 to 5.0 GHz. The experimentally determined attenuation per unit time given in Ref. 7 is approximated by the formula:

$$\text{Propagation loss} = 0.9 \; f^{1.9} \; dB/\mu s \qquad (7)$$

where f is the frequency of the surface waves in GHz. On the other hand, measurements cited in Ref. 8 more closely follow the equation:

$$\text{Propagation loss} = 1.25 \; f^{1.6} \; dB/\mu s \; . \qquad (8)$$

The discrepancy between the two measurements is believed to be caused partly by the fact that in Ref. 7 the loss due to "air loading" was excluded (i.e., the devices were measured in vacuum). The additional loss attributed to air loading was estimated to be 0.2 dB/μs at 1 GHz[6] and this loss must be added to that given by Eq. (7) for surface wave devices operated in air.

Equation (8) predicts the propagation attenuation for surface waves at 725 MHz to be 0.79 dB/μs. This agrees very well with the measured 0.80 dB/μs average loss per unit time between adjacent transducers. Three conclusions on transducer quality can be drawn from the fact that he measured loss between transducers appears to be entirely attributable to propagation attenuation:

(1) The four interdigital transducers have nearly identical conversion efficiency.

(2) The transducers are all well aligned with each other.

(3) The transducers are well aligned with the crystal axis.

An estimate of the increased insertion loss of a delay line due to misalignment of two adjacent transducers is given by:

$$\text{Loss} = 10 \ \log \ \frac{\sin^2 \pi \alpha \theta}{(\pi \alpha \theta)^2} \ (\text{dB}) \quad , \tag{9}$$

where θ is the angle of misalignment between the transducers and α is the normalized transducer width (i.e., the width of the transducer divided by the acoustic wavelength = 280 μm/4165 μm = 60.2). If 0.25 dB is assumed to be the minimum detectable insertion loss difference between transducers, then the insertion loss measurements indicate that the transducers are aligned to within better than 0.17 degrees of each other using the present step and repeat exposure technique and to within a fraction of a degree with the crystalline axis. Hence, by using careful substrate mounting techniques, well-aligned transducer patterns can be produced using the present slit-lens exposure system.

The frequency response of a surface wave delay line composed of two 4.5-period (9-finger) transducers spaced ≈ 0.5 cm apart is shown in Figure 16. The untuned insertion loss measurement was made using
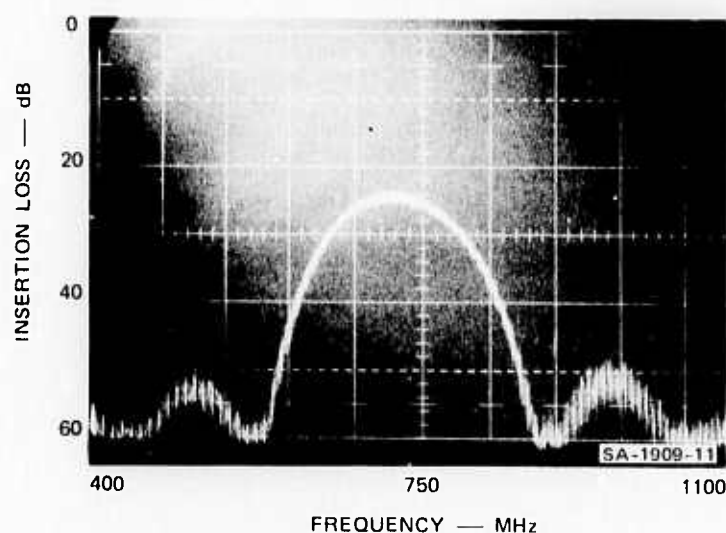

FIGURE 16   FREQUENCY RESPONSE OF SURFACE-WAVE
DELAY LINE—TYPE 1

38

a Hewlett-Packard network analyzer over a frequency range from 0.40 to 1.10 GHz. The minimum insertion loss was 23.5 dB and occured at 725 MHz. The delay line exhibited a bandwidth of 140 MHz (between the 5 dB points). The bandwidth predicted for an untuned delay line having two N-period transducers is

$$BW \ (6 \ dB) = \frac{f_o}{N} \quad , \tag{10}$$

where f_o is the fundamental frequency. For the case at hand, Eq. (10) predicts a bandwidth of 162 MHz. The upper and lower sidelobe level, seen in Figure 16 to be $\approx$ 26 dB down from the peak, was in accord with theoretical estimates of sidelobe level for transducers of uniform overlap (i.e., unapodized).

An alternative technique was used to analyze the performance of thes interdigital transducers. In this approach the electrical input impedance of thetransducer was measured near the fundamental operation frequency. Figure 17 shows the results of automatic network analyzer measurement of the real and imaginary components of input impedance taken at 50MHz intervals from 500 MHz to 1000 MHz on one of the interdigital transducers of the delay line. The reference plane (to which these measurements are referred) was taken at the end of the bond wire attached to the transducer, and hence the inductance of the bond wire must be included. An equivalent circuit model of the transducer and its parasitics is shown in the insert of Figure 17. The circuit includes: the parasitic series inductance L_s of the bond wire; stray capacitance to ground C_g from the transducer connections; series ohmic loss R_c of the transducer electrodes; and a series circuit composed of a frequency-dependent resistance R_a and reactance X_a attributed to electromechanical coupling to surface waves, plus a static capacitance C_T due to the interdigital electrode array. Smith[10] et al. have shown that this series transducer model accurately

39

PARASITIC ELEMENTS | SURFACE-WAVE TRANSDUCER

WHERE

L_S = Series inductance of the bond wires
C_g = Capacitance to ground of the transducer and pad
R_c = Ohmic resistance of the thin transducer electrodes
C_T = Transducer static capacitance
$R_a(\omega)$ = Acoustic radiation resistance of the transducer
$X_a(\omega)$ = Acoustic radiation reactance of the transducer, and equals zero at synchronism
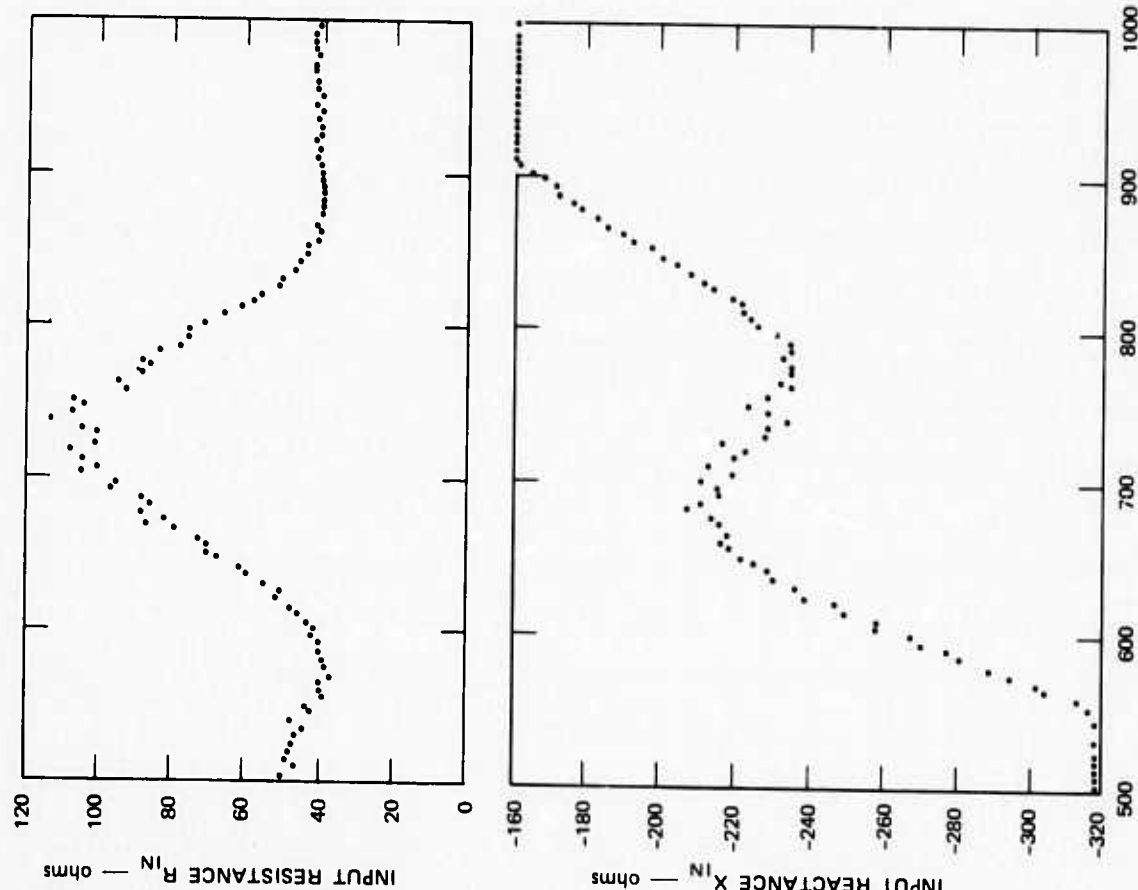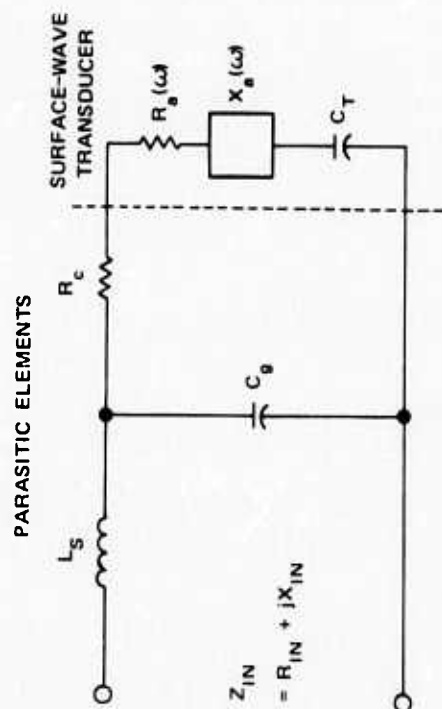
SA-1909-12

FIGURE 17   INPUT IMPEDANCE OF INTERDIGITAL SURFACE-WAVE TRANSDUCER

Equivalent series circuit representation of a surface-wave transducer shown in insert.

characterizes interdigital transducers in the 100-MHz frequency range and should be accurate at higher frequencies.

The transducer element values[*] at the synchronous frequency ω_o are predicted to be:

$$R_a(\omega_o) = \frac{4\ k^2}{\pi\omega_o C_s} \quad , \quad X_a(\omega_o) = 0 \tag{11}$$

$$C_T = NC_s = N\ (1 + \epsilon_r)\epsilon_o\ W, \tag{12}$$

where ϵ_r is the relative dielectric constant of the substrate[†] and ϵ_o is the dielectric constant of free space. The series ohmic resistance, R_c, for a transducer having a current distribution that varies linearly along the electrodes and is uniform across an electrode is given by:[9]

$$R_c = \frac{8}{3}\ \frac{R_s \alpha}{N} \quad , \tag{13}$$

where R_s is the sheet resistance of the metal electrodes in ohms per square. The calculated values of the circuit elements at 725 MHz for the transducer are: $R_a = 99.5\ \Omega$, $C_T = 0.57\,pF$ and $R_c = 53\ \Omega$ (using an estimated value of sheet resistance of aluminum of $1.66\ \Omega$ per square).

These theoretical values can be compared with the values derived from the input impedance measurements using the equivalent circuit model of Figure 17. Estimates of the parasitic components are $L_s \approx 10$ nH for the 0.8-cm long bond wire and $C_g \approx 0.15$ pF for the stray capacitance to ground. Substitution of these values into the equivalent circuit

---

[*] These values assume the transducer has equal width metal electrodes and gaps.

[†] For YZ $LiNbO_3$, $\epsilon_r = 50$.

41

and using the measured input impedance of R_{in} = 107 Ω, X_{in} = -222 Ω at the center frequency yield the following elements for the transducer: $R_a(\omega_d^o)$ = 100 Ω, C_T = 0.67 pF, and R_c = 60 Ω. These measurements agree quite closely with the theoretical predictions. The somewhat high background conductive loss of the electrodes is attributed in part to the thin aluminum used for the metallization.

The input impedance data show that a substantial portion of the insertion loss of the line was due to impedance mismatch between the circuit and the transducer and was not attributable to the transducer itself. In fact, the total mismatch loss of the line (i.e., both transducers) is 10.7 dB. The mismatch loss of one transducer is given by:

$$\text{Mismatch loss} = -10 \log_{10} (1 - \rho^2) , \qquad (14)$$

where ρ is the reflection coefficent at the input. The reflection coefficient for the transducer whose input impedance is shown in Figure 17 is ρ = 0.84.

It can be shown that if both transducers were tuned with lossless inductors, the insertion loss of the line would decrease about 9.5 dB to yield a minimum insertion loss value of $\approx$ 14 dB. This remaining 14 dB loss can be attributed to the 6 dB-bidirectionality loss of the transducers, the series conductive loss, the mismatch loss of the transducer, and the propagation losses.

The above test results show the transducers produced by the slit-lens exposure technique to be of high quality, well aligned with both the other transducers on the delay line and the crystal axis.

D. Experimental Evaluation of Type 2 Transducer Patterns (1.75 μ
   Interfinger Spacing and 1.15 GHz Center Frequency)

Measurements of insertion loss and input impedance (similar to those
made on the 725-MHz line) were made on two surface wave delay lines,
each having five interdigital transducer patterns spaced 0.32 cm apart.
The patterns have a periodicity of 3.50 ± 0.04 μm. When viewed under
a high power microscope, these patterns appear to be of good quality
and without broken or shorted electrodes. Figure 18 shows the RF
pulse delay characteristics of this delay line and the corresponding
insertion loss measured between adjacent transducers of 0.88 μs agrees
well with the calculated delay of 0.91 μs. The direct RF electromag-
netic feedtrhough pulse (the first pulse observed in each photograph)
was larger in these measurements than those made at 725 MHz because of
more closely spaced transducers (0.32 cm versus 0.5 cm) and higher
operating frequency (1.15 GHz). The small-pulsed signals observable
on the bottom three photographs at 0.88 μs intervals were caused by
the large RF feedthrough pulse being picked up by output transducers
that reexcited surface waves.

The difference in insertion loss between adjacent transducers is
3.9 dB or on the average 4.43 dB per μs of delay. This value is sub-
stantially above the experimental value derived from Eq. (8) of 1.67
dB per μs at 1.15 GHz. This discripancy was not explained by possible
loss due to small misalignment between transducers or misalignment
between the transducers and the crystal axis.

The untuned frequency response of the delay line consisting of
(non-adjacent) transducers spaced 0.64 cm apart was measured with the
Hewlett-Packard network analyzer. The device was remounted in the
fixture that gave reduced RF feedthrough. Results of this test displayed
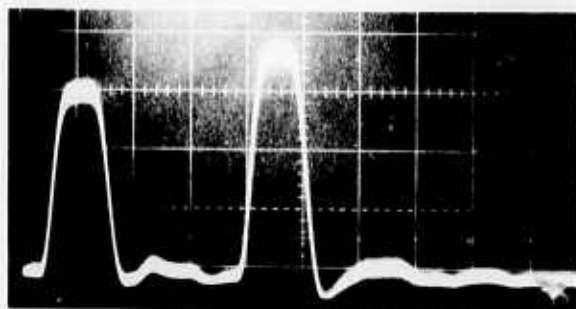
(a) INPUT TO
TRANSDUCER 1
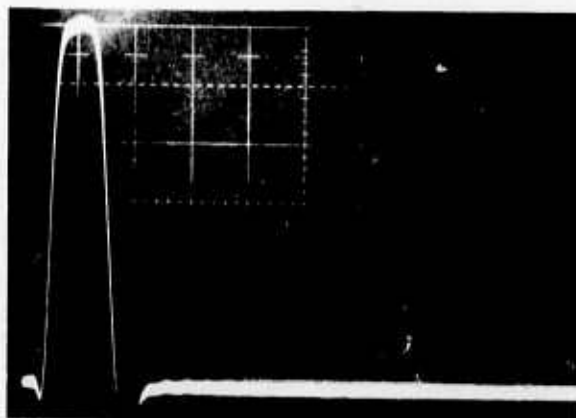
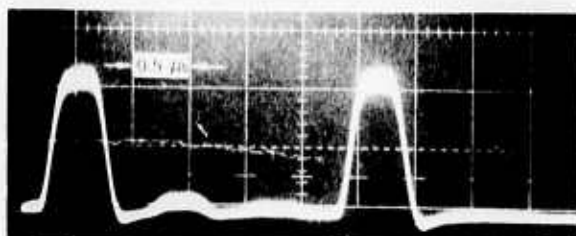(b) OUTPUT FROM
TRANSDUCER 2
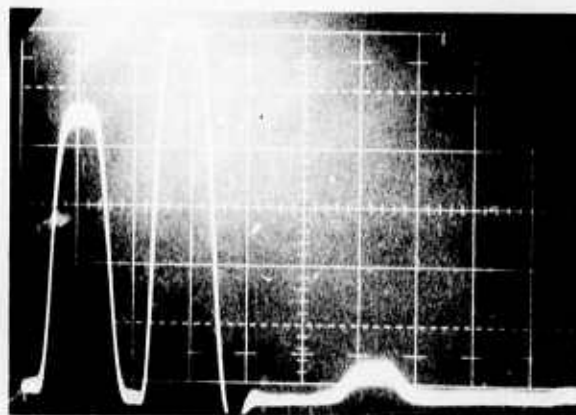
INSERTION LOSS
= 22.5 dB

(c) OUTPUT FROM
TRANSDUCER 3

INSERTION LOSS
= 26.5 dB

(d) OUTPUT FROM
TRANSDUCER 4

INSERTION LOSS
= 30.4 dB

TIME DELAY

SA-1909-13

FIGURE 18   RF PULSE TRANSMISSION THROUGH TYPE 2 SURFACE-WAVE
DELAY LINE AT 1.15 GHz

in Figure 19 show the delay line to have a minimum untuned insertion loss of 30 dB at a frequency of 1.15 GHz. The 6-dB bandwidth of the
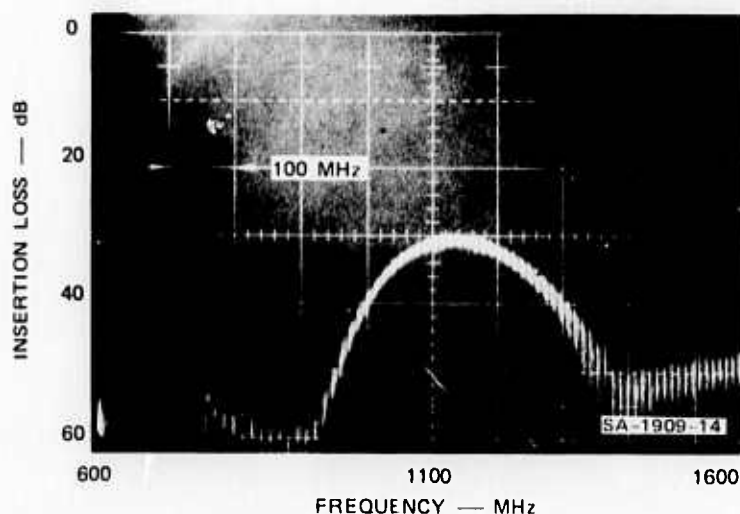

FIGURE 19   FREQUENCY RESPONSE OF SURFACE-WAVE
DELAY LINE—TYPE 2

delay line is 240 MHz and agrees well with the bandwidth of 256 MHz calculated from Eq. (10) at 1.15 GHz. The lower frequency sidelobe appears to be $\approx$ 26 dB below the minimum in insertion loss as expected; however, the upper sidelobe was obscured due to the direct electromagnetic feedthrough.

The input impedance of these 1.15 GHz center frequency transducers was measured using a network analyzer over the frequency range from 0.8 to 1.6 GHz. Figure 20 displays the input impedance versus frequency on a Smith chart (normalized to 50 Ω) for one transducer. The input impedance of the transducer was measured to be $R_{in} \equiv 150\ \Omega$, $X_{in} = -115\ \Omega$ at the synchronous frequency of 1.15 GHz. This measured

45

SA-1909-15

FIGURE 20   INPUT IMPEDANCE (SMITH PLOT) OF 1150 MHz
FUNDAMENTAL FREQUENCY INTERDIGITAL
SURFACE-WAVE TRANSDUCER

impedance can be used in conjunction with the equivalent circuit shown
in Figure 20 to determine the transducer and various parasitic element
values.   Performing the analysis yields the measured values of $R_a(\omega_o)$ =
79 Ω, C_T = 0.57 pF, R_c = 157 Ω, and C_g = 0.15 pF, assuming L_s to be
10 nH.   The theoretical element values were calculated using Eqs. (11),
(12), and (13) to be $R_a(\omega_o)$ = 62.6 Ω, C_T = 0.57 pF, and R_c = 79 Ω (assuming
R_s = 1.66 Ω per square). One observes that the measured transducer elements
$R_a(\omega_o)$ and C_T are in substantial agreement with theory; however, the
ohmic series loss of the transducer are much higher than expected and
might be caused by the larger sheet resistance of the thinner metalli-
zation used on this transducer.

The mismatch loss of this delay line has been determined from the
reflection coefficient (ρ = 0.66) of the transducers to be $\approx$ 5.0 dB.
Hence, tuning the line with a lossless inductor would reduce the inser-
tion loss 3.5 dB from the minimum measured 22.5 dB to 20 dB.   The trans-
ducer electrode loss, however, prevents the full 5.0 dB reduction in loss.

46

The tests of these microwave frequency interdigital transducers again demonstrate high quality of the device and the capabilities of the slit-lens exposure technique.

E.   Experimental Evaluation of Type 3 Transducer Patterns (0.68 μ Interfinger Spacing and 2.8 GHz Center Frequency)

Pulsed insertion loss measurements were carried out on several delay lines composed of a number of interdigital transducer patterns of 1.36 ± 0.04 μm electrode periodicity. The adjacent transducers were spaced $\sim$ 0.5 cm apart and aligned with both the crystal axes and the adjacent patterns. These transducers did exhibit some structural defects (i.e., broken electrodes) when viewed under a high power microscope, although several transducers had 9 out of 10 good electrodes. Figure 21 shows the microwave pulse delay characteristics of one delay line having 3 transducers, each composed of 4 electrode pairs when driven at 2.8 GHz. The input signal was applied to one end transducer and received at the two output transducers. In this instance the RF feedthrough pulse has been suppressed from the received signal by gating the local oscillator off at the time the feedthrough pulse would occur. The "untuned" insertion loss between adjacent transducers is 55 dB and the loss to the nonadjacent transducer is 67 dB. The 12-dB difference in loss between the transducers (or 8.3 dB/μs) appears to be mostly attributable to propagation loss. Using Eq. (8) the calculated loss at 2.8 GHz for surface waves on YZ LiNbO$_3$ should be 6.5 dB/μs. The discrepancy may be due to differences in transducer efficiencies or propagation loss mechanisms (beam steering, transducer tilting, or crystal polish). The delay measured was 1.45 μs between adjacent transducers, as expected.

(a) INPUT TO
    TRANSDUCER 1
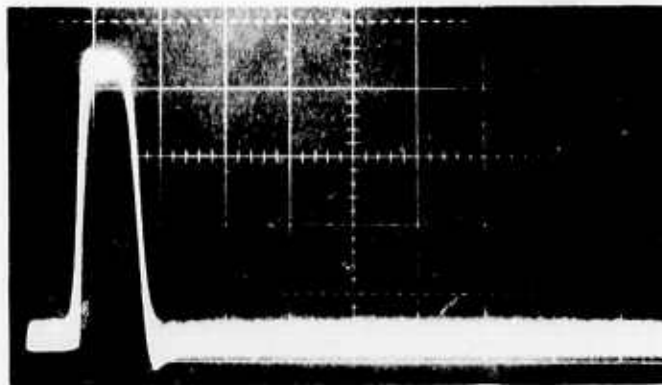
(b) OUTPUT FROM
    TRANSDUCER 2
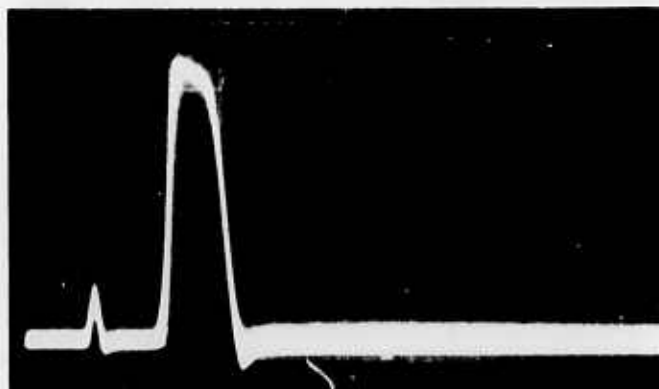
INSERTION LOSS
= 55 dB

1 μs

(c) OUTPUT FROM
    TRANSDUCER 3
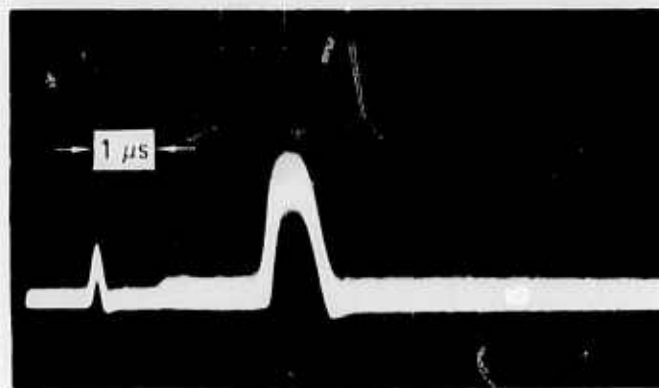
INSERTION LOSS
= 57 dB

TIME DELAY

SA-1909-16

FIGURE 21   RF PULSE TRANSMISSION THROUGH TYPE 3 SURFACE-WAVE
             DELAY LINE AT 2.8 GHz

The microwave test fixture used to mount this delay line did not allow accurate input impedance measurement, and hence the transducers could not be characterized in this way. However, the pulsed performance of the delay lines show the devices to function well even at this extremely high operating frequency.

VI   CONCLUSIONS AND RECOMMENDATIONS

Under this contract a projection electron-beam exposure system, based on an aperture slit-lens, was designed and built. It is capable of producing high resolution surface acoustic wave transducer patterns in electron-sensitive resist material. In parallel with the development of the slit-lens exposure system, thin-film techniques have been developed that use these image patterns to fabricate aluminum film interdigital transducers on Y-cut Z-propagating $LiNbO_3$. Several delay lines composed of these interdigital transducers have been fabricated, tested, and evaluated. The transducers worked well at frequencies as high as 2.8 GHz. These transducer patterns, having a periodicity of 1.36 μm, are believed to be some of the highest fundamental frequency surface wave transducers reported to date[2,3,4]   .

The test results on the lower frequency transducers of center frequency 725 MHz and 1.15 GHz illustrated the high quality of the interdigital transducer patterns. The measurements indicated that, by simple inductive tuning, insertion losses on the order of 14 dB at 725 MHz and 20 dB at 1.15 GHz could be achieved for surface wave lines having 1 μs delay. All the delay lines fabricated were relatively wide band, having ≈ 20 percent (6 dB) bandwidth about the center frequency and showing the (sin X)/X-type frequency response characteristic of unapodized transducers.

The surface wave transducers were further characterized by making input impedance versus frequency measurements near the fundamental frequency using a Hewlett Packard automatic network analyzer. The results of these measurements agreed quite well with the expected impedance values calculated by using the surface wave equivalent circuit[10] when the parasitic bond wire inductance and bond electrode capacitance to ground were taken into account.

51

Preceding page blank

The pulsed and CW insertion loss in conjunction with the input impedance measurements all attest to the quality of the interdigital transducers fabricated on this program by the slit-lens technique. It appears that this fabrication approach can be used to extend the frequency at which surface wave signal-processing devices function well into the microwave regime, 1 to 4 GHz, and possibly higher on high surface wave velocity material such as aluminum nitride. Further work should be done to establish the resolution limits of this technique and hence the frequency limits of the fabricated transducers.

The slit-lens exposure system is capable of making devices more complex than the simple delay lines fabricated thus far. Additional work in the following two areas would be invaluable for producing such devices as frequency filters, tapped delay lines, and matched filters that would operate at microwave frequencies. First, a technique of weighting the strength of the individual taps is needed (by either width weighting or overlap apodization), and, second, a means of accurately positioning the interdigital taps over large areas (by an external step and repeat technique) to produce long arrays is required. If these improvements are made to the existing exposure system, a very flexible tool for the fabrication of surface wave devices would result.

ACKNOWLEDGMENTS

REFERENCES

1. R.M. White and F.W. Voltmer, "Direct Piezoelectric Coupling to Surface Elastic Waves," Appl. Phys. Lett. Vol. 7, pp.314-316 (December 15, 1965).

2. A.N. Broers, E.G. Lean, and M. Hatzakis, "1.75 GHz Acoustic-Surface Wave Transducer Fabrication by an Electron Beam" Appl. Phys. Lett. Vol. 15, pp. 98-101 (August 1, 1965).

3. E.D. Wolf, W.E. Perkins, and P.J. Coane, "Device Fabrication with the Stereoscan," Proc. Cambridge Stereoscan Colloquim, pp. 99-106 (1970)

4. P. Hartemenn and C. Arnodo, "Rayleigh Wave Delay Line Using Two Grating Array Transducers at 2.55 GHz," Electronics Letters, Vol. 8, pp. 265-267 (May 18, 1972).

5. H.I. Smith, F.J. Bachner, and N. Efremow, "A High-Yield Photo-lithographic Technique for Surface Wave Devices," J. of the Electrochemical Soc. Vol. 118, pp. 821-825 (May 1971).

6. D.L. Spears and H.I. Smith, "X-Ray Lithography--A New High Reso-lution Replication Process," Solid State Technology, Vol. 15, pp. 21-26 (July 1972).

7. A.J. Slobodnik, Jr., P.H. Carr, and A.J. Budreau, "Microwave Frequency Acoustic Surface Wave Loss Mechanisms on $LiNbO_3$," J. Appl. Phys. Vol. 41, pp. 4380-4387 (October 1970).

8. E.H. Lean and C.G. Powell, "Optical Probing of Surface Acoustic Waves," Proc. IEEE, Vol. 58, pp. 1939-1947 (December 1970).

9. H. Gerard, M. Wauk, and R. Weglein, "Large Time-Bandwidth Product Microwave Delay Line," Second Semiannual Progress Report, Technical Report ECOM-0385-2 (October 1970).

10. W.R. Smith et al., "Analysis of Interdigital Surface Wave Trans-ducers by Use of an Equivalent Circuit Model," IEEE Trans. on Microwave Theory and Techniques, Vol. MTT-17, pp. 856-864 (November 1969).

11. R. Gans, "Electron Paths in Electron-Optical Systems," Z.Tech Physik, Vol. 18, pp. 41-48 (February 1937).

Preceding page blank

Appendix

FIRST-ORDER SLIT-LENS THEORY

Trajectory analysis for electrons traveling through the electro-static field of a slit-lens can be performed by using an approximation technique developed by Gans[11]. The assumptions for this technique are that the field can be approximated in piecewise fashion by linear segments. This method can be applied to the slit-lens by assuming that the slit-lens potential can be separated into two pieces, a preslit potential of Φ_o and a postslit potential of $\Phi_o + \Phi_o{}'z$. This assumption becomes exact in the limiting case where the width of the slit approaches zero, i.e., the narrow slit approximation.

Figure A-1 defines the symbols used in the following derivation: The off-axis distance of the ray for the field of a one-dimensional slit can be obtained by solving the paraxial ray equation,

$$y'' + \frac{\Phi'y'}{2\Phi} + \frac{\Phi''y}{2\Phi} = 0 \qquad (A-1)$$

For Ray 1 in Region I the solution is trivial:

$$y = y_o{}'(z - s_o) \qquad . \qquad (A-2)$$

For the transition zone between Regions I and II, Φ'' becomes infinite whereas Φ, Φ', y, and y' are all finite. Treating Φ and y as constants since they are continuous, we can integrate Eq. (A-1) across the slit.

$$\int_{z=0^-}^{z=0^+} y'' \, dz = - \int_{z=0^-}^{z=0^+} \left(\frac{\Phi'y'}{2\Phi} + \frac{\Phi''y}{2\Phi} \right) dz \qquad (A-3)$$

A-1

REGION I

REGION II

$\Phi = \Phi_o$

RAY 1

$\Phi = \Phi_o + \Phi_o'z$

y_1'

y_o

AXIS

y_o'

y_i'

y_i

z

y_o

RAY 2

y_o'

z_o

z_i

OBJECT
PLANE

SLIT-LENS PLANE
$z = 0$

IMAGE
PLANE
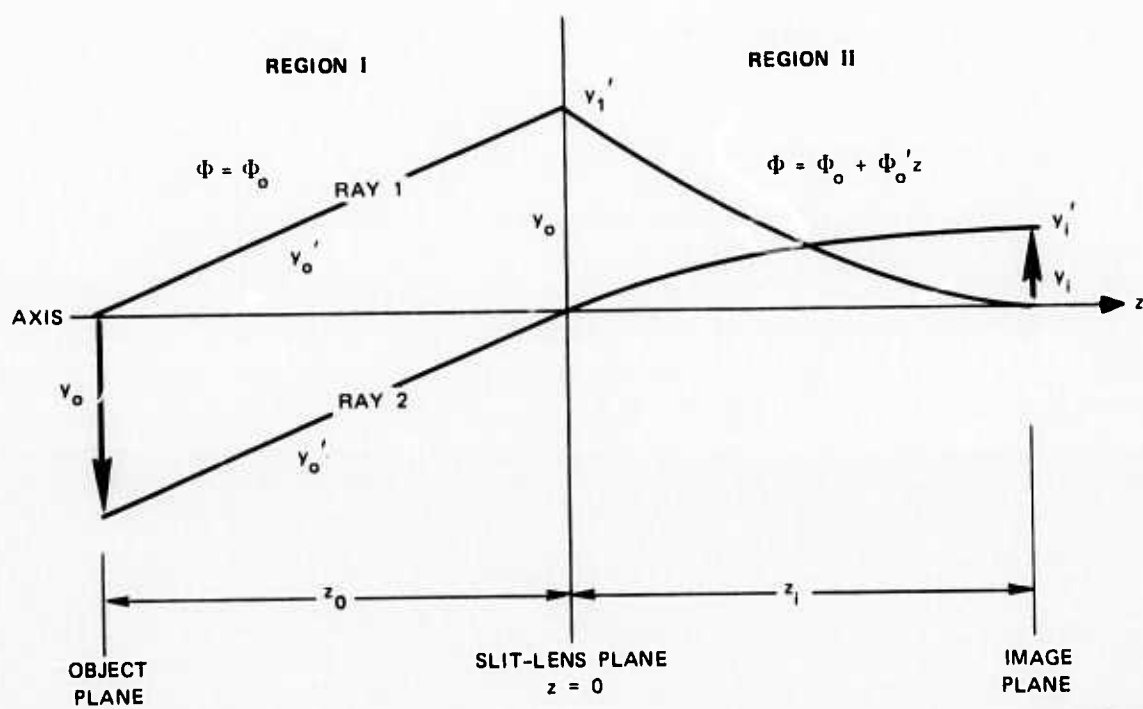
SA-1909-17

FIGURE A-1   SLIT-LENS TRAJECTORIES

A-2

$$y'_i - y'_o = - \frac{\left(\Phi'_{z=0^-} - \Phi'_{z=0^+} \right)}{2\Phi_o} \, y_o \qquad , \qquad (A-4)$$

or rewriting

$$y'_i - y'_o = \frac{- \Phi'_o y_1}{2\Phi_o} \qquad . \qquad (A-5)$$

In Region II, $\Phi'' = 0$. Using this condition Eq. (A-1) can be integrated to give

$$y = y_o + 2y'_i \; \frac{\Phi_o^{1/2}}{\Phi'_o} \; \left[\left(\Phi_o + \Phi'_o z \right)^{1/2} - \Phi_o^{1/2} \right] \quad . \quad (A-6)$$

Writing $\qquad \beta \equiv \Phi_o / \Phi'_o \qquad\qquad\qquad (A-7)$

and using Eqs. (A-2) and (A-5) to solve (A-6), we have

$$y = y'_o \left[2 \left(s_o - \beta \right) + \left(2\beta - s_o \right) \left(1 + z/\beta \right)^{1/2} \right] . \quad (A-8)$$

An image is formed at $z = x_i$ when $y = 0$. Rearranging Eq. (A-8) and solving for $z = s_i$:

$$s_i = 4\beta \left(\frac{\beta - s_o}{2\beta - s_o} \right)^2 - 1 \qquad . \qquad (A-9)$$

If we judiciously make $s_i = d$ (the distance from the substrate to the slit) so that focus occurs on the substrate and take $\Phi'_o \equiv \Phi_s / d$ where $\Phi_s \equiv$ the potential on the substrate with respect to the slit, we can solve Eq. (A-9) for the voltage ratio Φ_s / Φ_o:

$$\frac{\Phi_s}{\Phi_o} = \frac{3}{2} + \frac{2d}{s_o} + \left(\frac{9}{4} + \frac{2d}{s_o} \right)^{1/2} \qquad (A-10)$$

A-3

Since s_o is generally $\gg$ d, this reduces to:

$$\frac{\overset{\Phi}{s}}{\Phi_o} = 3 \qquad . \qquad (A\text{-}11)$$

The trajectory of Ray[2] can be used to determine y_i and hence the magnification. For this ray the equation in Region I becomes

$$y = y_o' z \quad ,$$

and the ray equation in Region II is

$$y = \frac{2y_o \beta}{s_o} \left(\left(1 + z/\beta \right)^{1/2} - 1 \right) \qquad . \qquad (A\text{-}12)$$

Solving for $y = y_i$ at $z = s_i$, we obtain the demagnification of the system

$$\frac{1}{M} = \frac{-y_o}{y_i} = \frac{s_o}{2\beta} - 1 = \frac{s_o \overset{\Phi}{s}}{2\Phi_o d} - 1 \quad . \qquad (A\text{-}13)$$

For $d \ll s_o$, the demagnification simplifies to:

$$\frac{1}{M} = \frac{3}{2} \frac{s_o}{d} \qquad . \qquad (A\text{-}14)$$

The depth of field can be calculated from Eq. (A-8) using $\beta = \Phi_o / \Phi_o' = \Phi_o z / \Phi_s$, differentiating

$$\frac{dy}{dz} = \frac{2y_o' \Phi_o}{\Phi_o} \left[\left(1 + \frac{\overset{\Phi}{s}}{\Phi_o} \right)^{1/2} - 1 \right] \qquad . \qquad (A\text{-}15)$$

For $s_o \gg d \; \Phi_s / \Phi_o \approx 3$,

$$\frac{dy}{dz} \approx \frac{2}{3} y_o' \qquad (A\text{-}16)$$

Using the Lagrange-Helmholtz relation to rewrite y'_o in terms of y'_i

$$y'_o \; y_o \; \Phi_o^{1/2} = y'_i \; y_i \; \Phi_i^{1/2} = y'_i \; y_i \; (\Phi_s + \Phi_o)^{1/2} \qquad (A-17)$$

Again, for $s_o \gg d$:

$$\frac{y'_i}{y'_o} = \frac{y_o}{2y_i} = \frac{1}{2M} \qquad (A-18)$$

$$\frac{dy}{dz} \approx \frac{4}{3} \; My'_i \qquad , \qquad (A-19)$$

or

$$\Delta z \approx \frac{3}{4} \; \frac{\Delta y}{My'_i} \qquad . \qquad (A-20)$$

This depth of field Δz is a factor of $3/4M$ larger than for the usual nonself-focusing lens, e.g., the Einzel lens.